Microporous and Mesoporous Materials

Bio-oils/FCC co-processing: Insights into the adsorption of guaiacol on Y zeolites with distinct acidity and textural properties

--Manuscript Draft--

Manuscript Number:	MICMAT-D-21-00362R1
Article Type:	Full length article
Keywords:	Keywords: Faujasite, guaiacol, adsorption, acidity, bio-oils co-processing
Corresponding Author:	Auguste Fernandes Universidade de Lisboa Instituto Superior Técnico: Universidade de Lisboa Instituto Superior Tecnico Lisbon, PORTUGAL
First Author:	João Miguel Silva, PhD
Order of Authors:	João Miguel Silva, PhD
	Maria Filipa Ribeiro, PhD
	Inês Graça, PhD
	Auguste Fernandes, PhD
Abstract:	The guaiacol adsorption capacity of several Y zeolites with different physicochemical properties was tested by performing breakthrough adsorption experiments, in order to investigate the guaiacol adsorption on Fluid Catalytic Cracking catalysts during bio-oils/FCC feedstocks co-processing. X-Ray diffraction, nitrogen sorption measurements and pyridine adsorption followed by Infrared Spectroscopy were used to determine the framework Si/Al ratio, the textural parameters, and finally the nature and amount of acid sites. Klinkenberg model was used to fit the experimental data and to obtain the guaiacol adsorption capacity and k a (overall coefficient of mass transfer) and K e (adsorption equilibrium constant) parameters, which are directly related to, respectively, kinetic and thermodynamic aspects. K e values, and so guaiacol adsorption, were observed to increase with the total number of Brønsted and Lewis acid sites on the zeolites, as well as with the amount of Na exchange. Conversely, mesoporosity increases the diffusion rate of guaiacol inside the zeolite structure, leading to higher k a values and decreasing guaiacol retention. Overall, data show that guaiacol adsorption on the FCC catalysts, and so its impact on the activity, might decrease with the catalyst age, owing to the changes on the FCC catalyst properties taking place during operation.

Bio-oils/FCC co-processing: Insights into the adsorption of guaiacol on Y zeolites with distinct acidity and textural properties

HIGHLIGHTS

- Adsorption of guaiacol on Y zeolites with distinct acidity and textural properties
- Zeolites with high Brønsted and Lewis acid sites present higher guaiacol adsorption
- High guaiacol adsorption for zeolites with high density of acid sites
- Large mesopores volume and external surface area give higher guaiacol diffusion rate
- Guaiacol adsorption capacity from breakthrough adsorption experiments

GA

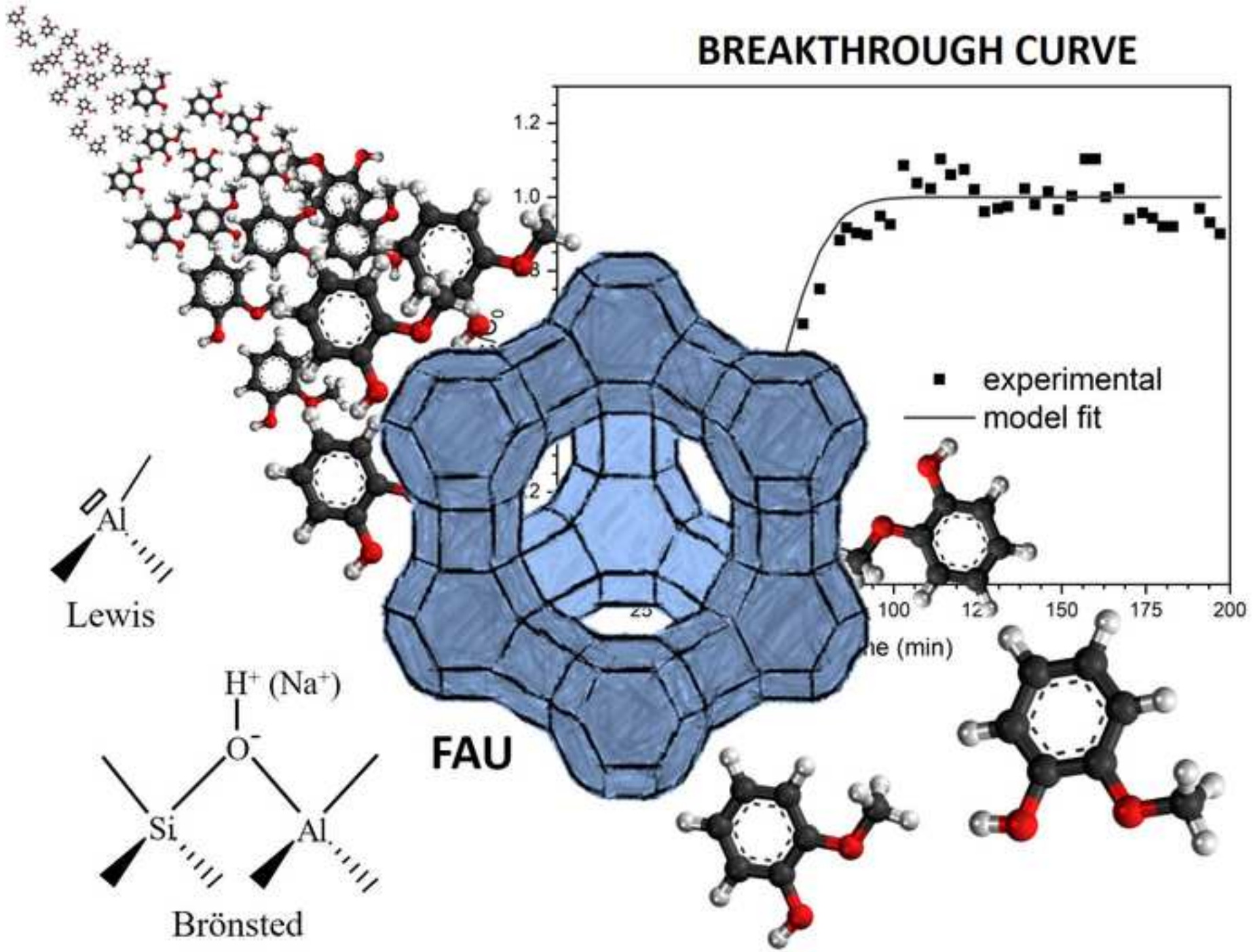
BREAKTHROUGH CURVE
1.2
1.0
experimental
model fit
100
150
175
200
Lewis
H+ (Na+)
O-
Si
Al
Brönsted
FAU

Bio-oils/FCC co-processing: Insights into the adsorption of guaiacol on Y zeolites with distinct acidity and textural properties

J. M. Silva[a,b], M. F. Ribeiro[a], I. Graça[c*], A. Fernandes[a*]

[a]Centro de Química Estrutural and Departamento de Engenharia Química, Instituto Superior Técnico, Universidade de Lisboa, Av. Rovisco Pais, P-1049-001 Lisboa, Portugal
[b]Área Departamental de Engenharia Química, Instituto Superior de Engenharia de Lisboa, Instituto Politécnico de Lisboa, Rua Conselheiro Emídio Navarro, 1, 1959-007 Lisboa, Portugal
[c]University of Aberdeen, School of Engineering, Fraser Noble Building, King's College, Aberdeen AB24 3UE, Scotland, United Kingdom

[*]**Corresponding authors:** Auguste Fernandes, auguste.fernandes@tecnico.ulisboa.pt, phone: (+351) 218419183/fax: (+351) 218419198; Inês Graça, i.graca@abdn.ac.uk, phone: (+44) (0)1224 273293

Abstract

The guaiacol adsorption capacity of several Y zeolites with different physicochemical properties was tested by performing breakthrough adsorption experiments, in order to investigate the guaiacol adsorption on Fluid Catalytic Cracking catalysts during bio-oils/FCC feedstocks co-processing. X-Ray diffraction, nitrogen sorption measurements and pyridine adsorption followed by Infrared Spectroscopy were used to determine the framework Si/Al ratio, the textural parameters, and finally the nature and amount of acid sites. Klinkenberg model was used to fit the experimental data and to obtain the guaiacol adsorption capacity and k_a (overall coefficient of mass transfer) and K_e (adsorption equilibrium constant) parameters, which are directly related to, respectively, kinetic and thermodynamic aspects. K_e values, and so guaiacol adsorption, were observed to increase with the total number of Brønsted and Lewis acid sites on the zeolites, as well as with the amount of Na exchange. Conversely, mesoporosity increases the diffusion rate of guaiacol inside the zeolite structure, leading to higher k_a values and decreasing guaiacol retention. Overall, data show that guaiacol adsorption on the FCC catalysts, and so its impact on the activity, might decrease with the catalyst age, owing to the changes on the FCC catalyst properties taking place during operation.

Keywords: Faujasite, guaiacol, adsorption, acidity, bio-oils co-processing

1. Introduction

In order to reduce the dependence on crude oil and decrease CO_2 emissions, traditional fossil fuels must be replaced by alternative fuels based on renewable sources, such as lignocellulosic biomass. Lignocellulosic biomass is currently one of the renewable sources of carbon that can be converted into liquids (bio-oils) able to be used as transportation fuels [1,2]. Furthermore, contrarily to petroleum, biomass presents the advantage of containing negligible amounts of sulphur, nitrogen and metals, and its balance of CO_2 is neutral. However, these wood-derived bio-oil fractions contain important amounts (up to 45 wt.%) of oxygenated compounds, such as carboxylic acids, aldehydes, alcohols, ketones, esters, ethers, phenols, furans and carbohydrates. The presence of significant amounts of oxygenated molecules in the bio-oils composition gives them some undesirable properties, such as high viscosity, thermal and chemical instability, lower miscibility with hydrocarbons and high tendency to form coke [3–5].

The co-processing of bio-oils with conventional Fluid Catalytic Cracking (FCC) feedstocks could be a promising short-term possibility to produce bio-fuels [6,7]. However, the high amounts of O-compounds in the bio-oils can limit their direct addition to the FCC petroleum-based feedstocks. Hence, a previous upgrading of the bio-oils, by reducing their oxygen content, is normally required and can be performed by hydrodeoxygenation (HDO). Nevertheless, phenolic molecules are difficult to remove by HDO, and usually remain after the treatment [8–10].

The impact of lignin derived phenols, such as phenol and guaiacol, on FCC catalysts during bio-oils/FCC feedstocks co-processing has been explored in the literature. These oxygenates can have a detrimental impact on FCC catalysts. In fact, studies performed with the two main components of FCC catalyst, HY and HZSM-5 zeolites, revealed that phenolic molecules significantly and quickly deactivate these zeolites [2,11–14], due to the phenolic compounds adsorption on both Brønsted and Lewis acid sites, together with coke molecules. However, questions remain regarding how zeolite physicochemical properties can influence phenolic molecules adsorption. This is especially important considering that FCC catalysts are a mixture with a distribution of ages and chemical and physical properties, and phenolic

compounds adsorption. Therefore, their impact on activity might change depending on the age of the catalyst particles [15].

Some works related to adsorption of phenol [16–18] and phenolic compounds such as ortho-nitrophenol, para-nitrophenol, meta-nitrophenol, and 2,4-dinitrophenol on synthetic zeolites have been published. It was found that, for the FAU structure, the capacity of adsorption increased with the Si/Al ratio, and that, for the same Si/Al ratio, Y zeolite was more effective than BEA and mordenite [18,19]. However, so far, it appears that no data are available concerning guaiacol adsorption on synthetic zeolites.

Therefore, in this work, guaiacol adsorption was studied over several Y zeolites presenting very distinct physicochemical properties, by performing breakthrough adsorption experiments, to analyze the potential for guaiacol to adsorb on the FCC catalyst during bio-oils/FCC feedstocks co-processing. The breakthrough adsorption experiments were carried out in order to: a) analyze the diffusion ability of guaiacol molecules within the zeolite porous structures, b) evaluate the strength of the interaction between the zeolites and the O-compound, and c) determine the maximum amount of guaiacol that can be retained on the zeolites, under the experimental conditions selected. The influence of the Si/Al ratio, the presence of extra-framework aluminium (EFAL) species and sodium, and the textural properties on the adsorption process were evaluated. Finally, the conclusions obtained from the experimental data were extrapolated to the conditions of the bio-oils/FCC feedstocks co-processing.

2. Experimental

2.1. Materials

Different commercial Y zeolites (FAU structure), namely DAY P (Degussa), $Na_{2.1}$USHY (Grace Davison), CBV 720, CBV 780, CBV 600, CBV 500 (all from Zeolyst), were used as adsorbents. CBV 500 sample, supplied in the ammonium form, was calcined at 500 ºC under a flux of dry air to be converted into its protonic form. Besides these commercial Y zeolites, another zeolite sample was prepared from the $Na_{2.1}$USHY zeolite by increasing its Na content. For that purpose, an ammonium form of this zeolite was firstly prepared by subjecting the zeolite to a three-time ion-exchange treatment under reflux with a 2 M ammonium nitrate aqueous solution, at 100 ºC, for 4 h, using a solution/zeolite ratio of 4 mL g^{-1}. After ion-exchange, the suspension was filtered under vacuum and the zeolite obtained was

washed with deionized water and dried overnight in an oven at 100 ºC. Then, a 4 h ion-exchange was performed (three times) at room temperature, with a solution/zeolite ratio of 4 $mL.g^{-1}$, by using a 2 M sodium nitrate aqueous solution. Finally, the zeolite sample obtained after Na-exchange was filtered under vacuum, dried overnight in an oven at 100 ºC and calcined at 500 ºC under a flux of dry air (referred to as $Na_{3.0}$USHY).

2.2. Characterization

Powder X-Ray diffraction (PXRD) patterns were recorded on a Bruker AXS Advance D8 diffractometer. Powder patterns were taken at room temperature between 5 and 40 º (2θ), with a scan step of 0.02 º and a time step of 6 s, using Cu-Kα radiation. NaCl was used as an internal standard and mixed with the samples. The unit cell parameter a_o was subsequently calculated from each diffractogram, using CELREF software and Si/Al ratio obtained using the empirical formula from [20].

Elemental chemical analyses were performed by inductively coupled plasma atomic emission spectrometry (ICP-AES), using a Philips ICP PU 7000 spectrometer, after acid digestion of the samples.

Particle size distribution curves of the zeolite samples were determined by Laser diffraction, using a CILAS 1064 particles size analyzer from Malvern.

Nitrogen adsorption measurements were carried out at -196 °C on a Micrometrics ASAP 2010 apparatus. Before adsorption, the fresh zeolite samples were degassed under vacuum at 90 °C for 1 h and then at 350 °C for at least 4 h. N_2 isotherms were used to determine the total porous volume (V_{total}), the micropores volume (V_{micro}), the external surface area (S_{ext}) and the pores size distribution (PSD) curves. The total pore volume was calculated from the adsorbed volume of nitrogen for a relative pressure P/P_0 of 0.97, whereas V_{micro} and S_{ext} were determined using the *t*-plot method. The mesopores volume (V_{meso}) was given by the difference V_{total} - V_{micro}. The PSD curves were calculated from the analysis of the isotherm adsorption branch based on the Barrett-Joyner-Halenda (BJH) algorithm.

The samples acidity was characterized by pyridine adsorption followed by FTIR spectroscopy, using a Nicolet Nexus spectrometer. The samples were pressed into thin wafers (10-20 mg cm^{-2}) and pre-treated in an IR quartz cell at 450 ºC for 2 h under secondary vacuum (10^{-6} mbar). The samples were then cooled down to 150 ºC and contacted with pyridine (P_{eq} = 1.5 mbar) during 10 min. Then, pyridine excess was removed for 30 min under secondary

vacuum and the IR spectra were recorded. The concentrations of Brønsted and Lewis sites able to retain the pyridine at 150 ºC were determined using the integrated areas of the bands at 1545 and 1455 cm^{-1}, respectively, and using extinction coefficients from literature [21].

The determination of theoretical adsorption energies for guaiacol on the Brønsted and Lewis acid sites of the zeolites, as well on the basic Si-ONa-Al sites, were estimated based on density functional theory (DFT) calculations, using the molecular modelling software Spartan v1.1.0. The Brønsted and Lewis acid sites were represented by simple clusters with formulas $AlSiOH_7$ and $AlSi_3O_3H_9$, respectively. For the Si-ONa-Al sites, a $AlSiONaH_6$ cluster was used. The hybrid B3LYP functional formalism and the 6-31G* atomic orbital basis set were employed to optimize the zeolite clusters, guaiacol geometry and cluster + adsorbed molecule configurations. The theoretical adsorption energies were calculated as $\Delta E_{adsorption}$ = E (cluster+adsorbed molecule) - E (cluster) - E (molecule gaseous phase).

2.3. Breakthrough adsorption experiments

The breakthrough adsorption experiments were carried out in a vertical Pyrex fixed-bed column at 150 °C, under atmospheric pressure, in the gas phase. Before each adsorption experiment, the zeolites were pre-treated at 200 °C under dry air flow (60 $mL.min^{-1}$) for 1 h and cooled down to the adsorption test temperature.

To keep the length of the zeolite bed constant (1.5 cm) around 120 mg of each zeolite were used. The feed was constituted by a solution of 1.2 wt.% of guaiacol (Sigma-Aldrich, 99%) in *n*-heptane (Sigma-Aldrich, 99%) and N_2, with a N_2/guaiacol mixture molar ratio of 9. N_2 was added to decrease the partial pressure of the guaiacol mixture and allows for its complete vaporization at the breakthrough adsorption experiment temperature. The mixture flow rate (3 $mL.h^{-1}$) was kept constant with a B|Braun compact perfusor. Variation of guaiacol vapor concentration during the adsorption experiments was monitored with a Chrompack CP 9001 gas chromatograph. The chromatographic column was a Varian CP SIL 5CB fused silica column with a dimethylpolysiloxane stationary phase and following dimensions: 10 m x 0.32 mm i.d., 0.25 µm film thickness. The operating conditions were as follows: an injector temperature of 275 ºC; a detector temperature of 260 ºC; N_2 was the make-up gas (27 mL min^{-1}) and the oven temperature program was 5 min at 50 ºC.

The breakthrough adsorption curve is usually expressed in terms of the outlet/inlet concentrations ratio ($C(t)/C_0$) as a function of the operation time (t). The model of Klinkenberg

[22–24], Eq. 1, was used to fit the guaiacol adsorption breakthrough curves obtained experimentally.

$$\frac{C}{C_0} = \frac{1}{2}\left[1 + \text{erf}\left(\sqrt{\tau} - \sqrt{\xi} + \frac{1}{8\sqrt{\tau}} + \frac{1}{8\sqrt{\xi}}\right)\right] \quad \text{Eq. 1}$$

with $\text{erf}(x) = \frac{2}{\sqrt{\pi}}\int_0^x e^{-t^2}dt$; $\tau = k_a\left(t - \frac{z}{u}\right)$; $\xi = k_a K_e \frac{z}{u}\left(\frac{1-\varepsilon}{\varepsilon}\right)$

and where erf(x) is the error function, k_a the overall mass transfer coefficient, K_e the adsorption equilibrium constant, z the bed height, u the gas velocity, t the time and ε the bed void fraction. The following parameters were considered: ε = 0.3; z = 1.5 cm and u = 728 cm min^{-1}. The model was adjusted to the experimental data by minimizing the sum of the squared absolute errors for C/C_0. Based on this, k_a and K_e values were determined for each zeolite. The maximum adsorption capacity of the zeolites for guaiacol, Q_T (mmol g^{-1}), was also estimated from the model fitted curves, according to Eq. 2.

$$Q_T = \frac{\left(\int_0^{t_{saturation}} 1dt - \int_{t_{breakthrough}}^{t_{saturation}} \frac{C(t)}{C_0}dt\right) \times F_0}{m}, \quad \text{Eq. 2}$$

where breakthrough time ($t_{breakthrough}$) corresponds to the initial detection of the adsorbate at the adsorber outlet, i.e. the minimum time required to cross the adsorbent bed, saturation time ($t_{saturation}$) is the point when the maximum capacity of retention of the adsorbent is reached, F_0 the entry molar flux of guaiacol and m the mass of zeolite used. However, $t_{breakthrough}$ and $t_{saturation}$ times were replaced by $t_{5\%}$ and $t_{95\%}$ times (times required to desorb 5 and 95 % of the adsorbate respectively; also calculated from the model fitting), since these later parameters are normally preferred as they are more reliable. Finally, the breakthrough adsorption slope was determined for each zeolite, by considering a linear adjustment $C(t)/C_0$ versus time within the interval $t_{5\%}$ and $t_{95\%}$.

3. Results and discussion

3.1. Characterization

The main physicochemical characteristics of the different adsorbents used in this study are reported in Table 1. All the samples are well crystalline materials with a FAU structure. The framework Si/Al_{IV} ratio calculated for each sample from the PXRD patterns are reported in Table 1, together with the unit cell formula (obtained from chemical analysis and PXRD results), the Na content, the global Si/Al and the particles size. The accuracy of the framework Si/Al_{IV} determined by PXRD was corroborated by comparing the values obtained with framework Si/Al_{IV} from ^{29}Si NMR found in the literature for the same commercial Y zeolites [25]. The amount of EFAL (extra framework Al) species per unit cell was obtained by the difference of the total Al content (from global Si/Al ratio) and the framework Al content (framework Si/Al_{IV} ratio). Hydrogen content was then calculated to balance negative charges (together with Na species), in order to obtain a neutral unit cell formula. From the Table 1, it can be seen that the samples present a very large range of global Si/Al (2.6-100), framework Si/Al_{IV} ratio (3.7-40), EFAL species contents (0-47.8) and different Na content.

TABLE 1

Nitrogen isotherms and PSD curves obtained for all the samples are shown in Figure 1 (all the isotherms have been shifted vertically for sake of clarity). Table 2 gives the corresponding textural parameters, namely pore sizes (in the mesopores region), external surface area S_{ext} and pores volume (V_{micro} and V_{meso}). Basically, two groups of FAU zeolites can be distinguished: one group corresponding to samples essentially microporous (isotherm of type I with a horizontal plateau at high relative p/p_0), with no or very weak mesopores contribution, and another group corresponding to microporous materials with an important contribution of mesopores (isotherms I with a hysteresis loop at high p/p_0). Logically, the first group, consisting of $Na_{2.1}$USHY, $Na_{3.0}$USHY, CBV 500 and DAY P (see Figure 1, open symbols), presents low external surface area (S_{ext}< 40 m^2 g^{-1}) and small mesopores volume (V_{meso}< 0.10 cm^3 g^{-1}).

FIGURE 1

On the other hand, the second group containing the remaining samples (CBV 720, CBV 780 and CBV 600, Figure 1, closed symbols), shows higher external surface area (> 55 m^2 g^{-1}) and larger mesopores volume (> 0.13 cm^3 g^{-1}). The presence of substantial mesoporosity in the later samples could be attributed to the fact that those materials had been all subjected to a dealumination process (in order to increase the framework Si/Al_{IV} ratio), as they present a rather high value (> 5) when compared with the less dealuminated samples (Si/Al_{IV} < 5). Interestingly, DAY P sample, which is a highly dealuminated sample, does not present any significant mesoporosity. Additionally, all the samples show micropores volume values in the range 0.24-0.34 cm^3 g^{-1}, typical for this type of materials. Moreover, while free EFAL species samples present relatively high micropores volumes (0.30-0.33 cm^3 g^{-1}), the presence of EFAL species in the other samples slightly decreases the micropores volume (0.24-0.29 cm^3 g^{-1}). This effect is more pronounced for CBV 600 sample, which is the one presenting the highest EFAL species content (0.24 cm^3 g^{-1} for 47.8 EFAL species per unit cell).

TABLE 2

Table 2 also shows the quantitative results obtained from pyridine adsorption, namely the amount of both Brønsted (B) and Lewis (L) acid sites able to retain pyridine molecule at 150 ºC under vacuum. In Figure 2, the amount of total, Brønsted and Lewis acid sites as a function of, respectively, global Si/Al, framework Si/Al_{IV} and the amount of EFAL species per unit cell, is shown. The total acidity (B+L) naturally follows the global Si/Al ratio of the different samples (see Figure 2-A), i.e., the higher the global Si/Al ratio, the lower the total acidity. The following total acidity amount order was observed: DAY P (Si/Al = 100) << CBV 780 (40) << CBV 720 (15) < CBV 600 (2.6), $Na_{2.1}$USHY (2.8), $Na_{3.0}$USHY (2.8) < CBV 500 (2.9).

On the other hand, Brønsted acidity can also be directly correlated with the framework Si/Al_{IV} ratio, as it can be seen in Figure 2-A. DAY P and CBV 780 are the materials that present the highest Si/Al_{IV} ratios (respectively 100 and 40) and logically present the lower amount of Brønsted sites, respectively 24 and 39 µmol g^{-1}. $Na_{2.1}$USHY, $Na_{3.0}$USHY and CBV 500, with Si/Al_{IV} of about 3.7-4.0, have the highest amount of Brønsted acid sites, with the two first

having a slightly lower value because of the presence of compensating Na^+ cations. CBV 720 and CBV 600 present an intermediate Brønsted value, as their Si/Al_{IV} ratio is about 9-16.

FIGURE 2

Concerning Lewis acid sites, here again it can be seen that the amount of Lewis sites follows the amount of EFAL species in the unit cell (Figure 2-B). However, CBV 600 sample, with an amount of 47.8 EFAL per unit cell, does not have much more Lewis acid sites than, for example, CBV500 sample (14.4 EFAL). A possible explanation could be that some Lewis sites might not be accessible to pyridine molecules, probably because of some hindrance caused by the presence of a very large amount of EFAL species in this sample.

All the adsorbents used in this work have a FAU structure, which is usually accessible to aromatic molecules with relatively large kinetic diameters, owing to the presence of supercages characterized by 12-membered rings (12-MR) with an open diameter of 7.4 Å. Through DFT calculations using the software Spartan, a kinetic diameter of 6.6 Å was estimated for guaiacol, which might indicate that the adsorption of guaiacol occurs preferentially on the supercages of the Y zeolites. In addition, it is also well-known that guaiacol interacts with both Brønsted and Lewis acid sites [14]. Theoretical adsorption energies calculated from Spartan software show that the interaction of guaiacol with Lewis acid sites (-108 kJ mol^{-1}) is stronger than with Brønsted acid sites (-88 kJ mol^{-1}). Interestingly, the theoretical adsorption energy of guaiacol on basic Na-exchanged zeolite framework sites was found to be -104 kJ mol^{-1}. Being similar to that estimated for Lewis acid sites, this might anticipate that Na presence also favors guaiacol adsorption.

3.2. Adsorption performance

Illustrative breakthrough curves, corresponding to the adsorption of 1.2 wt.% of guaiacol in *n*-heptane, obtained for DAY P and $Na_{2.1}$USHY samples, are presented in Figure 3. The results (amount of adsorbed guaiacol Q_T, breakthrough curves slopes, $t_{5\%}$ and $t_{95\%}$) extracted from the fitting curves are presented in Table 3, together with parameters k_a and K_e

also obtained from the model fit. The amount of guaiacol adsorbed by each sample was also confirmed by thermogravimetric measurements.

TABLE 3

FIGURE 3

Guaiacol breakthrough results show that all the samples reach a guaiacol adsorption equilibrium. However, from the different curves obtained, and also from the parameters extracted from the experimental fittings, one can distinguish once again two main groups. The first one (Group I) corresponds to samples DAY P (illustrated in Figure 3-A), CBV 720, CBV 780 and CBV 600 and is defined by the following features: small $t_{5\%}$ (< 30 min) and $t_{95\%}$ (< 50 min) and a very small difference between $t_{5\%}$ and $t_{95\%}$, demonstrated by a steep breakthrough curve slope ($\geq$ 0.043 min^{-1}, see Table 3). On the other hand, the second group (Group II), corresponding to samples CBV 500, $Na_{2.1}$USHY (illustrated in Figure 3-B) and $Na_{3.0}$USHY, can be defined by longer $t_{5\%}$ ($\geq$ 35 min) and $t_{95\%}$ ($\geq$ 77 min), resulting in a gentler breakthrough curve slope (< 0.025 min^{-1}). The direct consequence is the final guaiacol capacity that is very different from one group to the other: 1.05 mmol g^{-1} or less for the first group and 1.51 mmol g^{-1} or more for the second group.

Concerning the parameters k_a and K_e obtained from the Klinkenberg model, one can see that samples with a higher guaiacol adsorption capacity (Group II) have higher adsorption equilibrium constants ($K_e > 11x10^3$), while samples having a poorer guaiacol adsorption (Group I) present lower K_e values ($< 7x10^3$). Indeed, a very good linear correlation can be obtained by simply plotting the amount of guaiacol adsorbed, Q_T, as a function of K_e (see Figure 4), clearly showing that guaiacol adsorption onto FAU samples is essentially ruled by thermodynamics considerations. In the next section, it will be shown how FAU zeolites properties can explain this result. Concerning the overall coefficient of mass transfer (k_a), this

expresses how fast guaiacol molecules diffuse through the zeolite porous system. It can be seen in Table 3 that zeolites of Group I present higher k_a values (1.65-3.70 min^{-1}) than those belonging to Group II (0.69-1.10 min^{-1}). This means that diffusion of guaiacol is much faster on DAY P, CBV 720, CBV 780 and CBV 600 zeolites than on CBV 500, $Na_{2.1}$USHY and $Na_{3.0}$USHY zeolites, which correlates well with the slopes estimated for the breakthrough adsorption curves (Figure 5). Indeed, the lower the k_a value, the smoother the slope of the breakthrough curve, meaning a higher difference between $t_{5\%}$ and $t_{95\%}$. It is well known that molecules diffusion within the pores of a zeolite mainly takes place through the interaction with pore walls. Thus, the stronger the guaiacol adsorption to the pore walls of the zeolites, the lower the ability for the guaiacol molecules to diffuse through the zeolite porous system, which explains the lower k_a values (lower slopes values) for the zeolites of Group II.

FIGURE 4

FIGURE 5

3.3. Guaiacol adsorption vs zeolite properties

3.3.1. Sodium influence

With the purpose of studying the effect of the presence of sodium in zeolites framework on the guaiacol adsorption, zeolites $Na_{2.1}$USHY, $Na_{3.0}$USHY and CBV 500 were chosen, as they present similar physicochemical properties, except for the amount of Na. The two first zeolites are the only ones presenting Na in their framework as compensating cation, as it can be seen in Table 1. Na content on FCC catalysts can typically range from 0.2 to 0.5 wt.% upon exposure to the Na-containing FCC feedstocks. Considering the maximum value of 0.5 wt.% and the fact that the FCC catalysts usually contain 10-40 wt.% of Y zeolite in their formulations [15], the Na content on the pure zeolite can range from about 1 to 5 wt.%. Therefore, 2 and 3

wt.% of Na were chosen as representative amounts. It can be observed that presence of Na in the zeolite structure (up to 3 wt.%) seems to increase the guaiacol adsorption. This is not strange considering that the theoretical adsorption energy of guaiacol is higher on the basic Na-exchanged zeolite framework sites (-104 kJ mol^{-1}) than on the Brønsted acid sites (-88 kJ mol^{-1}). Indeed, Beutel *et al.* reported, by employing ^{1}H and ^{29}Si MAS NMR spectroscopy, that hydrogen bonding of phenol to the oxygen atoms of the zeolite is not the only interaction between phenol and Na-X zeolite. Of the same importance is the interaction of phenol aromatic ring with either Na^{+} cations or oxygens of zeolite supercages [26]. Some other studies also demonstrated similar phenol interaction with exchanged cations and zeolite oxygens [27,28].

3.3.2. Si/Al ratio influence

Zeolites, which are porous crystalline aluminosilicates, are formed by SiO_4 and AlO_4 tetrahedra connected by oxygen atoms, and their hydrophilic/hydrophobic character will depend essentially on the Si/Al framework ratio. It is generally accepted that for Si/Al < 10, zeolites are hydrophilic, i.e. water can interact easily with compensating cations (protons, etc.), while for Si/Al > 10, they turn hydrophobic because of the presence of non-polar ≡Si-O-Si≡ bridging groups [29]. Several studies have investigated the application of synthetic zeolites for the adsorption of phenolic compounds from wastewater and noticed the improvement of adsorption capacity with increased hydrophobicity [16,17,30,31]. In our case, the amount of guaiacol adsorbed onto the different FAU adsorbents as a function of Si/Al ratio and percentage of Al is illustrated in Figure 6. As it can be seen, the adsorption of guaiacol is favored using FAU zeolites with a low Si/Al ratio of about 4 (high number of aluminum atoms), i.e., zeolites with a rather hydrophilic character. This shows the importance of the number of framework and extra framework Al for the adsorption of guaiacol, in absence of an adsorption competition with water. Although this later condition is necessary, it is not enough to explain why CBV 600 sample is less efficient to adsorb guaiacol, although it has the same global Si/Al ratio as, for example, CBV 500 sample. This will be analyzed later in this paper.

FIGURE 6

3.3.3. Acid sites and EFAL species

From Figure 6 (B), one could see that the amount of Al in the zeolites plays a crucial role in the adsorption of guaiacol. Normally, zeolites present two types of Al species: Al species that are incorporated on the zeolite framework and account for the Brønsted acidity, and extra framework Al species. These extra framework (EFAL) Al species (octahedral, oligomers species or tri-coordinated Al) present in FAU structures are known to be responsible for the Lewis acidity of zeolites. Therefore, if guaiacol adsorption generally increases with the total number of Al, this is the same as saying that a higher guaiacol retention is expected for samples with a higher total amount of Brønsted and Lewis acid sites, which is indeed observed in Table 3. Following our findings concerning the estimated theoretical adsorption energies, it seems reasonable that both Brønsted and Lewis acid sites are responsible for the adsorption of guaiacol on the different FAU adsorbents. In fact, when plotting the evolution of the amount of guaiacol adsorbed as a function of the number of Brønsted acid sites (Figure 7), an increase in the amount of guaiacol retained on the zeolites can be seen with the Brønsted acidity. Figure 8 shows the amount of guaiacol adsorbed as a function of Lewis acidity (A) and EFAL species (B). Indeed, it also seems that guaiacol adsorption capacity follows both the Lewis acidity and EFAL amounts. However, in this latter case, the guaiacol adsorption passes through a maximum for CBV 500 sample, which is followed by a decrease for CBV 600. This result is unexpected considering that CBV 600 zeolite is the sample presenting the highest amount of EFAL species or Lewis acid sites, which were observed by DFT calculations to have a higher adsorption energy for guaiacol. The behavior of CBV 600 sample can be easily explained, taking into account the accessibility of the acid sites to the guaiacol molecules, which might be partially hindered by the large amount of EFAL species present in this sample. This conclusion is also supported by the previous observation on the underestimation of the Lewis acid sites by pyridine adsorption.

FIGURE 7

FIGURE 8

3.3.4. Textural parameters influence

Figure 9 shows the amount of guaiacol adsorbed (Q_T) on the various zeolites as a function of the mesoporous volume (V_{meso}), together with the linear relationship between V_{meso} and external surface area S_{ext}. When all the samples are compared, with exception of DAY P, the zeolites with a relatively high V_{meso} (> 0.10 $cm^3\ g^{-1}$) adsorb less guaiacol (< 1.10 mmol g^{-1}). This is quite surprising, considering that higher mesoporous volumes should lead to more space available to adsorb the bulky guaiacol molecules. Therefore, a higher guaiacol retention should be expected for the samples presenting an enhanced mesoporous volume. However, it is also known that the presence of mesopores in combination with micropores in zeolites is responsible for an increase in the diffusion rate of the guaiacol molecules inside the zeolite structure [2]. Indeed, according to the breakthrough curves slopes and k_a in Table 3, samples presenting improved mesoporous volume and external surface area are those for which a sharp slope and higher k_a values (higher diffusion rates) were found. Therefore, the increase in the diffusion rate generated by the higher mesoporous volume seems to prevail over the increase in space, in what concerns the guaiacol adsorption on the zeolites. In the case of the microporous volume, this one is generally similar for all the zeolite samples, except for CBV600 which presents a lower microporous volume. As previously mentioned, the high number of EFAL species on this sample might partially block its porous structure, decreasing the micropores volume, the accessibility to the acid sites and, consequently, reducing the guaiacol adsorption.

FIGURE 9

Overall, these results demonstrate that for acidic zeolites the total number of Brønsted and Lewis acid sites is the most important parameter that governs the amount of guaiacol adsorbed. Nevertheless, the presence of mesoporosity also seems to have an impact on the

guaiacol adsorption, as it increases the diffusion rate of guaiacol molecules. In addition, adsorption of guaiacol is increased if protons are exchanged by Na as compensating cations. Considering the properties of the catalyst used in the FCC process, these results can be extrapolated to the conditions of the bio-oils/FCC feedstocks co-processing. The equilibrium catalyst circulating in the FCC unit is composed by a mixture of catalyst particles with different ages and different chemical and textural properties [15]. Typically, the fresh ultra-stable Y (USY) zeolite used in the process has a low Si/Al framework ratio of 5. However, even though this USY catalyst is produced by controlled dealumination and presents an increased hydrothermal stability, it still undergoes further dealumination when submitted to the consecutive regeneration steps [32,33]. As a result, Al atoms are released from the zeolite framework, leading to an increase in the Si/Al framework ratio to 5-20. Consequently, this causes a reduction in the number of Brønsted acid sites, an increase in the Lewis acid sites (as EFAL species are generated) and an increase in the mesoporous volume of the zeolite. Therefore, adsorption of guaiacol is expected to be higher on fresh FCC catalyst, due to lower Si/Al ratio, higher amount of Brønsted acid sites and moderate quantity of EFAL species. On the other hand, an aged FCC catalyst with a higher Si/Al, a lower number of Brønsted acid sites and a higher number of EFAL species (that may hinder adsorption as observed) should adsorb a lower number of guaiacol molecules during co-processing. Additionally, the higher mesopores volume of the aged FCC catalyst would also facilitate the diffusion of the guaiacol molecules, decreasing their retention inside the zeolite structure. On the other hand, it is also known that Na content on the FCC catalysts also increases with circulation time, due to the presence of Na-containing compounds in the feed [15]. As observed, this increase in the sodium content should increase the amount of guaiacol adsorbed. However, Na passivators are used on the FCC catalyst to avoid the protons being exchanged by the Na, which would minimize this effect. Thus, the different guaiacol adsorption capacities for the fresh and aged FCC catalysts would certainly have implications on the poisoning effect of guaiacol during bio-oils/FCC feedstocks co-processing. Given the expected higher retention of guaiacol on the fresh FCC catalyst, a higher detrimental effect should be anticipated in this case.

4. Conclusions

Various FAU zeolites, with different framework Si/Al ratios (ranging from 3 to 100), amounts of Brønsted and Lewis acid sites and textural parameters, were tested for the adsorption of guaiacol. The parameters obtained from experimental guaiacol adsorption breakthrough curves and subsequent model fitting, i.e. guaiacol capacity, adsorption equilibrium constant (K_e), coefficient of mass transfer (k_a), $t_{5\%}$ and $t_{95\%}$, breakthrough curve slopes showed a direct correlation with the physicochemical properties of the zeolites. All the results show that materials with low Si/Al ratio (about 4) and high total amount of both Brønsted and Lewis acid sites (> 600 μmol g^{-1}) present a higher guaiacol adsorption, as well as higher K_e values, confirming theoretical adsorption energies calculations. On the other hand, zeolites with higher mesoporous volumes or external surface area led to a higher diffusion rate within the zeolite structure (higher k_a values), decreasing guaiacol retention. In addition, the replacement of protons by sodium atoms as compensating cations was also observed to increase guaiacol adsorption. Taking into account the changes that take place on the FCC catalyst properties during operation, it is expected that the poisoning effect of guaiacol during bio-oils/FCC feedstocks co-processing is attenuated with the increase of the catalyst age.

Acknowledgments

The authors thank Fundação para a Ciência e a Tecnologia (FCT, Portugal) for financial funding (UIDB/00100/2020 and UIDP/00100/2020). Fernandes also thanks FCT for researcher contract hiring (DL No. 57/2016 regulation).

References

[1] S.-Y. No, Application of bio-oils from lignocellulosic biomass to transportation, heat and power generation - A review, Renew. Sustain. Energy Rev. 40 (2014) 1108–1125. https://doi.org/http://dx.doi.org/10.1016/j.rser.2014.07.127.

[2] I. Graça, A.M. Carmo, J.M. Lopes, M.F. Ribeiro, Improving HZSM-5 resistance to phenolic compounds for the bio-oils/FCC feedstocks co-processing, Fuel. 140 (2015) 484–494. https://doi.org/http://dx.doi.org/10.1016/j.fuel.2014.10.002.

[3] Q. Lu, W.-Z. Li, X.-F. Zhu, Overview of fuel properties of biomass fast pyrolysis oils, Energy Convers. Manag. 50 (2009) 1376–1383.

https://doi.org/http://dx.doi.org/10.1016/j.enconman.2009.01.001.

[4] M. Badawi, J.-F. Paul, S. Cristol, E. Payen, Guaiacol derivatives and inhibiting species adsorption over MoS2 and CoMoS catalysts under HDO conditions: A DFT study, Catal. Commun. 12 (2011) 901–905. https://doi.org/http://dx.doi.org/10.1016/j.catcom.2011.02.010.

[5] J.D. Martínez, A. Veses, A.M. Mastral, R. Murillo, M. V Navarro, N. Puy, A. Artigues, J. Bartrolí, T. García, Co-pyrolysis of biomass with waste tyres: Upgrading of liquid bio-fuel, Fuel Process. Technol. 119 (2014) 263–271. https://doi.org/http://dx.doi.org/10.1016/j.fuproc.2013.11.015.

[6] I. Graça, J.M. Lopes, H.S. Cerqueira, M.F. Ribeiro, Bio-oils Upgrading for Second Generation Biofuels, Ind. Eng. Chem. Res. 52 (2013) 275–287. https://doi.org/10.1021/ie301714x.

[7] S.D. Stefanidis, K.G. Kalogiannis, A.A. Lappas, Co-processing bio-oil in the refinery for drop-in biofuels via fluid catalytic cracking, WIREs Energy Environ. 7 (2018) e281. https://doi.org/https://doi.org/10.1002/wene.281.

[8] A. Centeno, E. Laurent, B. Delmon, Influence of the Support of CoMo Sulfide Catalysts and of the Addition of Potassium and Platinum on the Catalytic Performances for the Hydrodeoxygenation of Carbonyl, Carboxyl, and Guaiacol-Type Molecules, J. Catal. 154 (1995) 288–298. https://doi.org/http://dx.doi.org/10.1006/jcat.1995.1170.

[9] V.N. Bui, G. Toussaint, D. Laurenti, C. Mirodatos, C. Geantet, Co-processing of pyrolisis bio oils and gas oil for new generation of bio-fuels: Hydrodeoxygenation of guaïacol and SRGO mixed feed, Catal. Today. 143 (2009) 172–178. https://doi.org/http://dx.doi.org/10.1016/j.cattod.2008.11.024.

[10] E. Furimsky, Hydroprocessing challenges in biofuels production, Catal. Today. 217 (2013) 13–56. https://doi.org/http://dx.doi.org/10.1016/j.cattod.2012.11.008.

[11] I. Graça, J.M. Lopes, M.F. Ribeiro, M. Badawi, S. Laforge, P. Magnoux, F. Ramôa Ribeiro, n-Heptane cracking over mixtures of HY and HZSM-5 zeolites: Influence of the presence of phenol, Fuel. 94 (2012) 571–577. https://doi.org/http://dx.doi.org/10.1016/j.fuel.2011.11.033.

[12] I. Graça, A. Fernandes, J.M. Lopes, M.F. Ribeiro, S. Laforge, P. Magnoux, F. Ramôa Ribeiro, Effect of phenol adsorption on HY zeolite for n-heptane cracking: Comparison with methylcyclohexane, Appl. Catal. A Gen. 385 (2010) 178–189. http://internal-pdf//Applied Catalysis A General 385 (2010) 178–189-

3558158849/Applied Catalysis A General 385 (2010) 178–189.pdf.

[13] I. Graça, A. Fernandes, J.M. Lopes, M.F. Ribeiro, S. Laforge, P. Magnoux, F. Ramôa Ribeiro, Bio-oils and FCC feedstocks co-processing: Impact of phenolic molecules on FCC hydrocarbons transformation over MFI, Fuel. 90 (2011) 467–476. http://internal-pdf//Fuel 90 (2011) 467–476-1059295232/Fuel 90 (2011) 467–476.pdf.

[14] R.T.J. Gerards, A. Fernandes, I. Graça, M.F. Ribeiro, Towards understanding of phenolic compounds impact on Ni- and V-USY zeolites during bio-oils co-processing in FCC units, Fuel. 260 (2020) 116372. https://doi.org/https://doi.org/10.1016/j.fuel.2019.116372.

[15] R. Sadeghbeigi, Fluid Catalytic Cracking Handbook: Design, Operation and Troubleshooting of FCC Facilities, 2nd Ed., Gulf Professional Publishing, 2000.

[16] M. Ahmaruzzaman, Adsorption of phenolic compounds on low-cost adsorbents: A review, Adv. Colloid Interface Sci. 143 (2008) 48–67. https://doi.org/http://dx.doi.org/10.1016/j.cis.2008.07.002.

[17] L. Damjanovíc, V. Rakíc, V. Rac, D. Stosíc, A. Auroux, The investigation of phenol removal from aqueous solutions by zeolites as solid adsorbents, J. Hazard. Mater. 184 (2010) 477–484. https://doi.org/http://dx.doi.org/10.1016/j.jhazmat.2010.08.059.

[18] N.A.S. Amin, J. Akhtar, H.K. Rai, Screening of combined zeolite-ozone system for phenol and COD removal, Chem. Eng. J. 158 (2010) 520–527. https://doi.org/http://dx.doi.org/10.1016/j.cej.2010.01.042.

[19] B. Koubaissy, G. Joly, P. Magnoux, Adsorption and Competitive Adsorption on Zeolites of Nitrophenol Compounds Present in Wastewater, Ind. Eng. Chem. Res. 47 (2008) 9558–9565. https://doi.org/10.1021/ie8001777.

[20] D.W. Breck, E.M. Flanigen, Synthesis and properties of Union Carbide zeolites L, X and Y, in: Mol. Sieves, Society of Chemical Industry, 1968: pp. 28–38.

[21] S. Morin, P. Ayrault, N.S. Gnep, M. Guisnet, Influence of the framework composition of commerical HFAU zeolites on their activity and selectivity in m-xylene transformation, Appl. Catal. A Gen. 166 (1998) 281–292. https://doi.org/http://dx.doi.org/10.1016/S0926-860X(97)00263-9.

[22] A. Klinkenberg, Heat Transfer in Cross-Flow Heat Exchangers and Packed Beds, Ind. Eng. Chem. 46 (1954) 2285–2289. https://doi.org/10.1021/ie50539a021.

[23] Y. Taamneh, R. Al Dwairi, The efficiency of Jordanian natural zeolite for heavy metals removal, Appl. Water Sci. 3 (2013) 77–84. https://doi.org/10.1007/s13201-012-0061-2.

[24] A. Chatterjee, S. Schiewer, Multi-resistance kinetic models for biosorption of Cd by raw and immobilized citrus peels in batch and packed-bed columns, Chem. Eng. J. 244 (2014) 105–116. https://doi.org/https://doi.org/10.1016/j.cej.2013.12.017.

[25] P.P. Pescarmona, K.P.F. Janssen, C. Delaet, C. Stroobants, K. Houthoofd, A. Philippaerts, C. De Jonghe, J.S. Paul, P.A. Jacobs, B.F. Sels, Zeolite-catalysed conversion of C3 sugars to alkyl lactates, Green Chem. 12 (2010) 1083–1089. https://doi.org/10.1039/b921284a.

[26] T. Beutel, M.J. Peltre, B.L. Su, Interaction of phenol with NaX zeolite as studied by 1H MAS NMR, 29Si MAS NMR and 29Si CP MAS NMR spectroscopy, Colloids Surfaces A Physicochem. Eng. Asp. 187–188 (2001) 319–325. https://doi.org/http://dx.doi.org/10.1016/S0927-7757(01)00647-1.

[27] D. Smart, T. Curtin, T.F. O'Dwyer, Influence of Cation-Exchanged Copper on the Adsorption of Phenol onto Zeolite Beta, Adsorpt. Sci. Technol. 32 (2014) 635–646. https://doi.org/10.1260/0263-6174.32.8.635.

[28] H. Jabraoui, I. Khalil, S. Lebègue, M. Badawi, Ab initio screening of cation-exchanged zeolites for biofuel purification, Mol. Syst. Des. Eng. 4 (2019) 882–892. https://doi.org/10.1039/C9ME00015A.

[29] N.Y. Chen, Hydrophobic properties of zeolites, J. Phys. Chem. 80 (1976) 60–64. https://doi.org/10.1021/j100542a013.

[30] M. Khalid, G. Joly, A. Renaud, P. Magnoux, Removal of Phenol from Water by Adsorption Using Zeolites, Ind. Eng. Chem. Res. 43 (2004) 5275–5280. https://doi.org/10.1021/ie0400447.

[31] N. Jiang, R. Shang, S.G.J. Heijman, L.C. Rietveld, High-silica zeolites for adsorption of organic micro-pollutants in water treatment: A review, Water Res. 144 (2018) 145–161. https://doi.org/https://doi.org/10.1016/j.watres.2018.07.017.

[32] H.S. Cerqueira, G. Caeiro, L. Costa, F. Ramôa Ribeiro, Deactivation of FCC catalysts, J. Mol. Catal. A Chem. 292 (2008) 1–13. https://doi.org/https://doi.org/10.1016/j.molcata.2008.06.014.

[33] F. Hernández-Beltrán, J.C. Moreno-Mayorga, M. de Lourdes Guzmán-Castillo, J. Navarrete-Bolaños, M. González-González, B.E. Handy, Dealumination–aging pattern of REUSY zeolites contained in fluid cracking catalysts, Appl. Catal. A Gen. 240 (2003) 41–51. https://doi.org/https://doi.org/10.1016/S0926-860X(02)00433-7.

TABLES

Table 1. Physicochemical characteristics of the different Y zeolites used in this study.

Zeolites	Unit cell formula	Na (wt.%) [a]	Si/Al [b]	Si/Al_{IV} [c]	Si/Al_{IV} NMR [d]	Particle size (µm) [e]
DAY P	$H_{1.9}Al_{1.9}Si_{190.1}O_{384}$	0.0	100	-	-	6.2
$Na_{2.1}$USHY	$Na_{17.5}H_{20.9}Al_{38.4}Si_{153.6}O_{384}$; 16.5 EFAL	2.1	2.8	4.0	-	4.4
$Na_{3.0}$USHY	$Na_{24.6}H_{16.3}Al_{40.9}Si_{151.1}O_{384}$; 13.1 EFAL	3.0	2.8	3.7	-	-
CBV 720	$H_{11.3}Al_{11.3}Si_{180.7}O_{384}$; 0.8 EFAL	0.0	15	16	22	4.4
CBV 780	$H_{4.9}Al_{4.7}Si_{187.3}O_{384}$	0.0	40	40	40.4	-

CBV 600	$H_{18.9}Al_{18.8}Si_{173.2}O_{384}$; 47.8 EFAL	0.0	2.6	9.2	9.6	4.6
CBV 500	$H_{40}Al_{40}Si_{152}O_{384}$; 14.4 EFAL	0.0	2.9	3.8	4.6	-

[a]from elemental analysis; [b]from manufacturer; [c]framework Si/Al_{IV} ratio calculated from the unit cell parameter a_0 (PXRD experiments), using Breck–Flanigen equation [20], [d]from P. P. Pescarmona *et al.* [25], [e]measured by laser diffraction.

Table 2. Textural and acidity properties of the Y zeolite samples.

Sample	Pore size (Å)	S_{ext} ($m^2.g^{-1}$)	Pore volume ($cm^3\,g^{-1}$)[a]		Acidity (μmol g^{-1})[b]		
			V_{micro}	V_{meso}	Brønsted	Lewis	Total
DAY P	58	36	0.30	0.06	24	23	47
$Na_{2.1}$USHY	159	15	0.29	0.04	416	373	789
$Na_{3.0}$USHY	162	17	0.29	0.06	453	225	678
CBV 720	242	84	0.31	0.21	281	122	403
CBV 780	240	83	0.33	0.18	39	101	140
CBV 600	159	56	0.24	0.13	271	396	667
CBV 500	161	33	0.28	0.08	628	343	971

[a]V_{micro} from *t*-plot, $V_{meso} = V_{total} - V_{micro}$; [b]from pyridine desorption at 150 °C.

Table 3. $t_{5\%}$, $t_{95\%}$, Q_T, breakthrough curves slopes, k_a and K_e parameters obtained from Klinkenberg model fittings [22].

Sample	$t_{5\%}$ (min)	$t_{95\%}$ (min)	Slope (min^{-1})	Q_T (mmol g^{-1})	k_a (min^{-1})	K_e ($x10^3$)
DAY P	10	19	0.100	0.40	3.70	3.0
$Na_{2.1}$USHY	49	86	0.024	1.82	1.04	13.8
$Na_{3.0}$USHY	50	87	0.024	1.86	1.10	14.1
CBV 720	22	43	0.043	0.87	1.65	6.6
CBV 780	17	34	0.053	0.68	1.79	5.2
CBV 600	29	47	0.050	1.05	2.60	7.9
CBV 500	35	77	0.021	1.51	0.69	11.4

Figures captions

Figure 1. Nitrogen sorption isotherms (A) and PSD curves (B) for the different zeolite samples (□ DAY P, ∇ $Na_{3.0}$USHY, o $Na_{2.1}$USHY, Δ CBV 500 ◄ CBV 720, ■ CBV 780 and ● CBV 600).

Figure 2. Total (Δ) and Brønsted (○) acidity as a function of, respectively, global and framework Si/Al (A); Lewis (□) acidity as a function of EFAL species (B).

Figure 3. Breakthrough curves (guaiacol adsorption) obtained for DAY P (A) and $Na_{2.1}$USHY (B) samples.

Figure 4. Amount of guaiacol adsorbed (Q_T) as a function of parameter K_e.

Figure 5. Slope of the breakthrough adsorption curves as a function of parameter k_a.

Figure 6. Amount of guaiacol adsorbed as a function of global Si/Al ratio (A) and Al molar percentage (B).

Figure 7. Amount of guaiacol adsorbed (Q_T) as a function of Brønsted acidity.

Figure 8. Amount of guaiacol adsorbed (Q_T) as a function of Lewis acidity (A) and EFAL species (B).

Figure 9. Amount of guaiacol adsorbed Q_T as a function of the mesopores volume V_{meso} (inset: V_{meso} as a function of external surface area, S_{ext}).

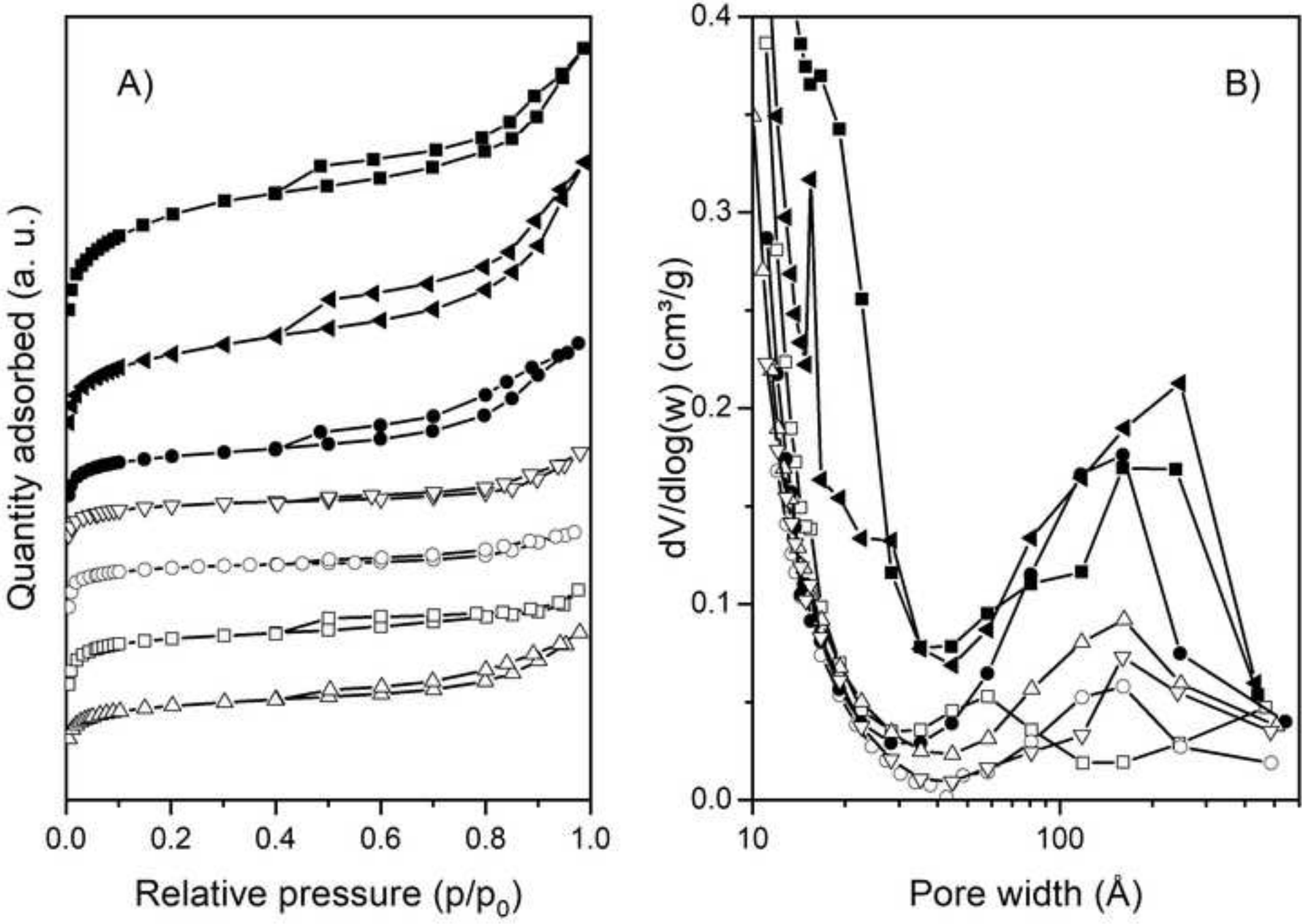

Fig2a

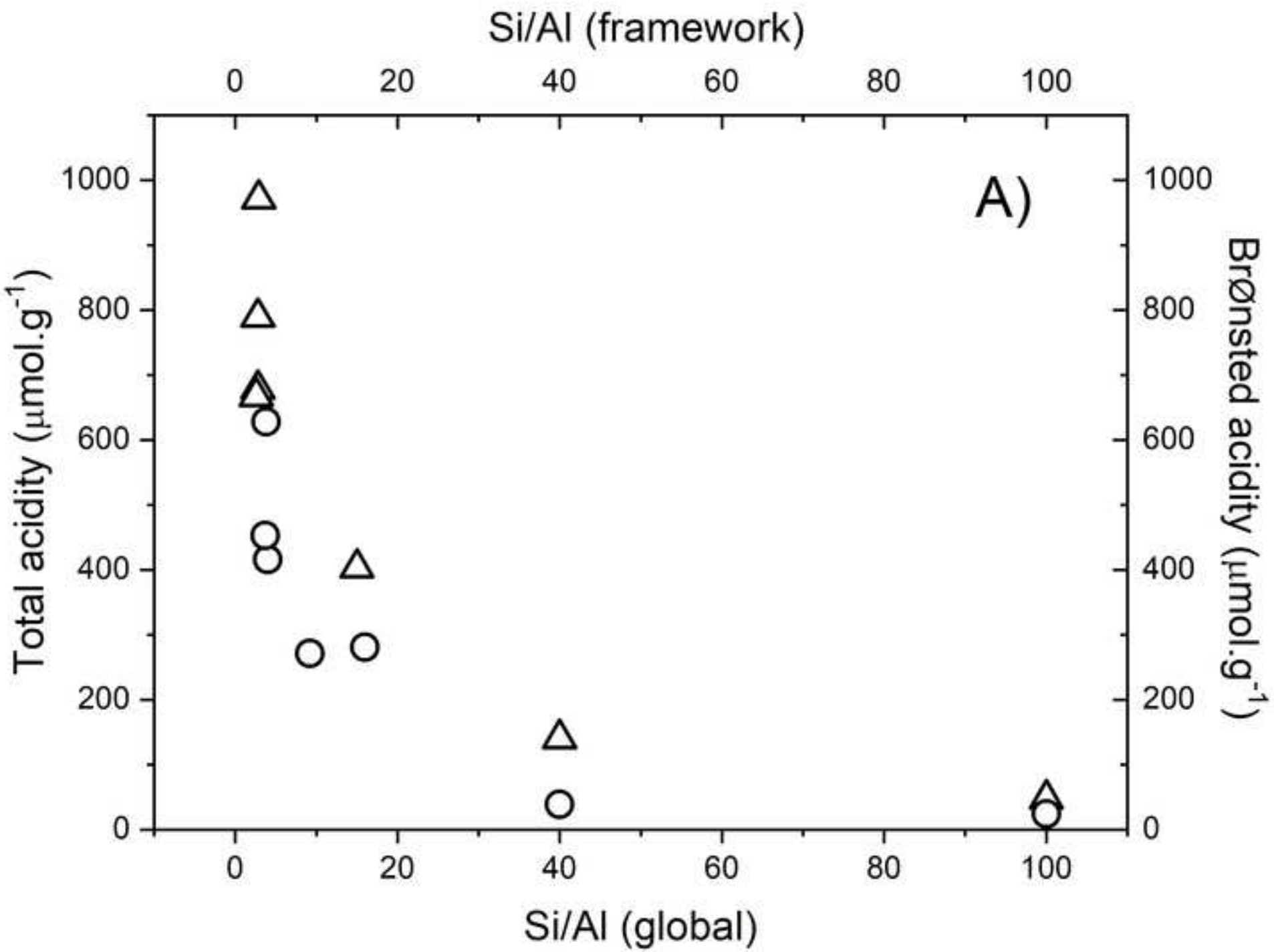

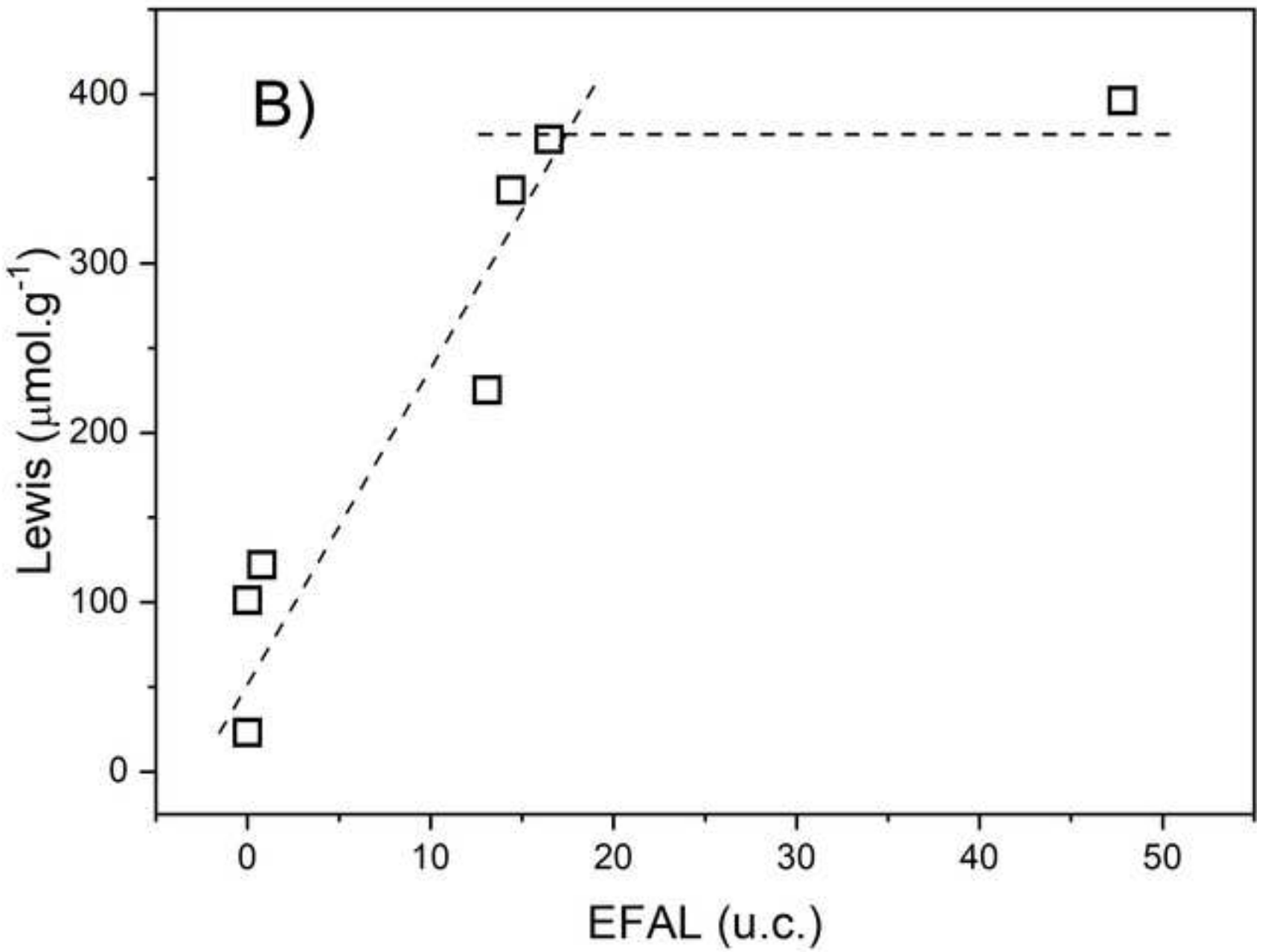

Fig3a

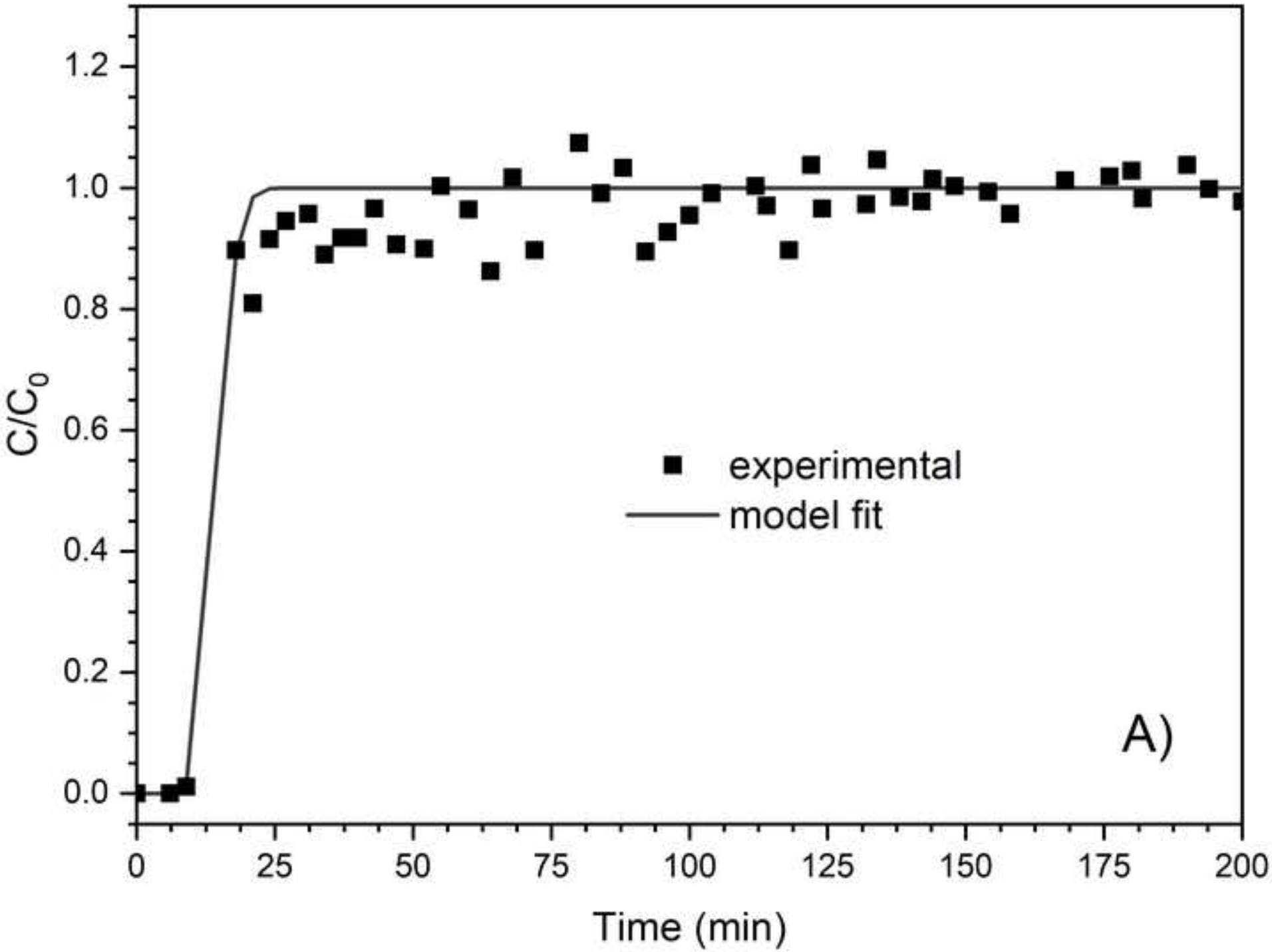

Fig3b

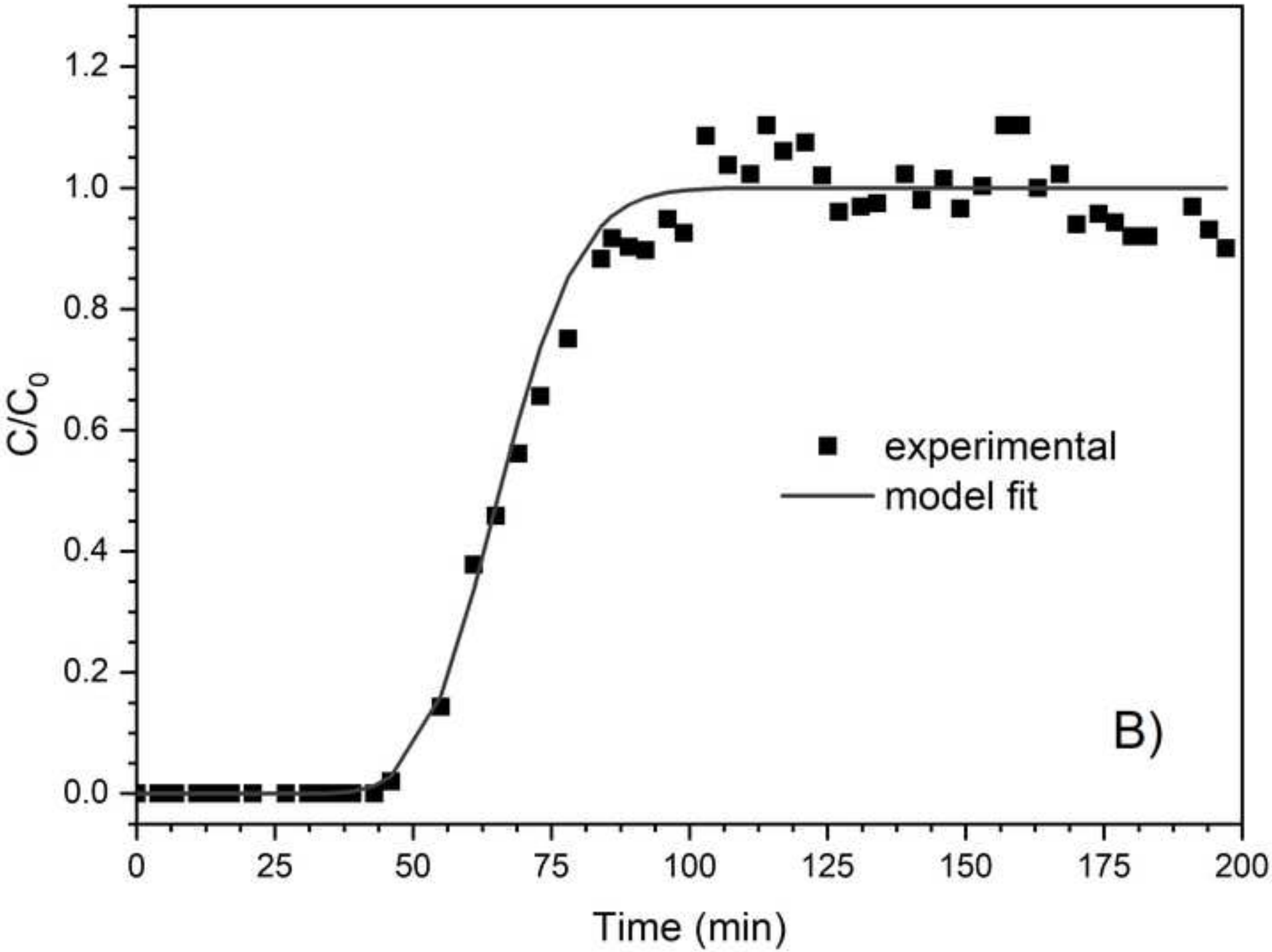

Fig4

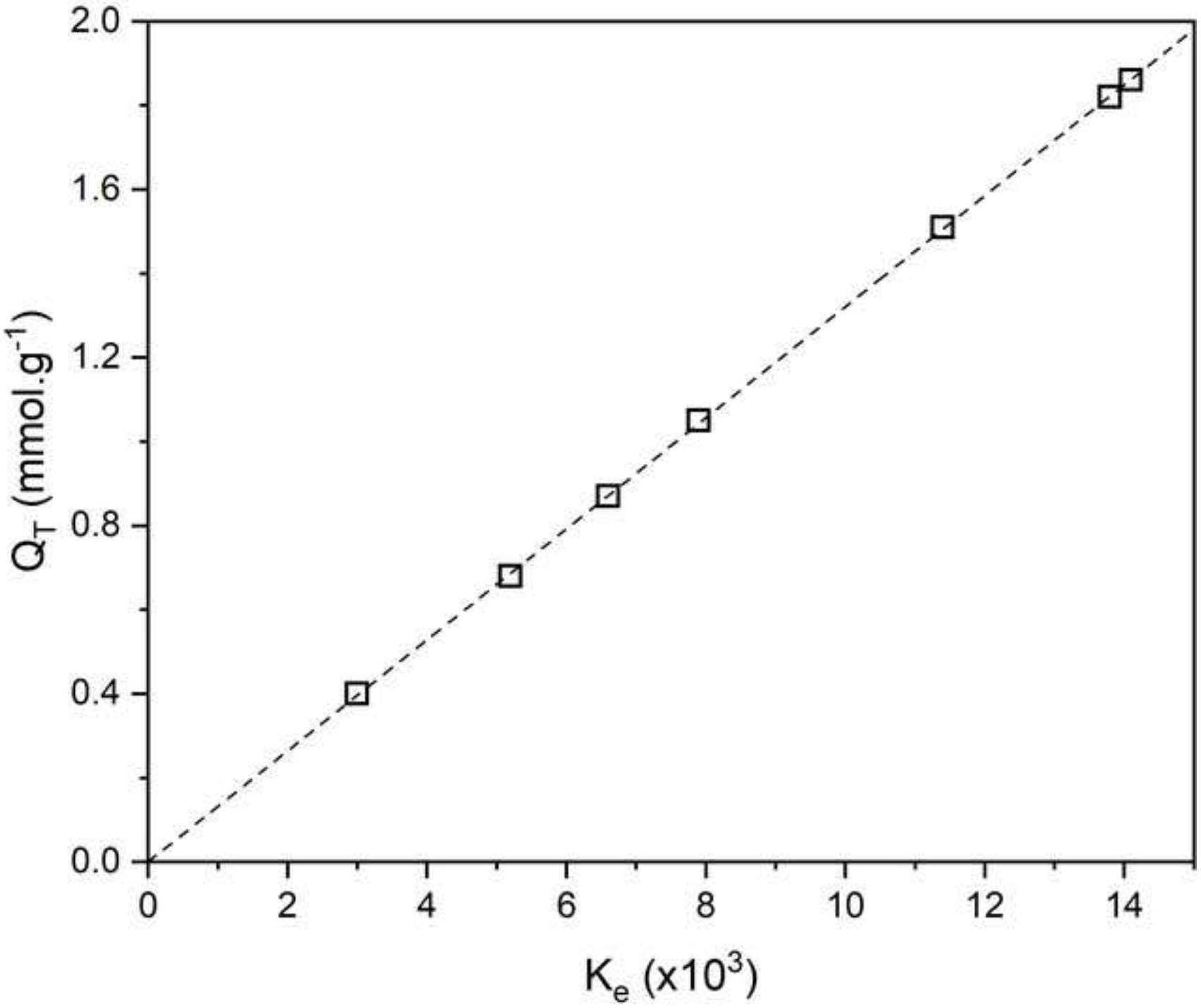

Fig5

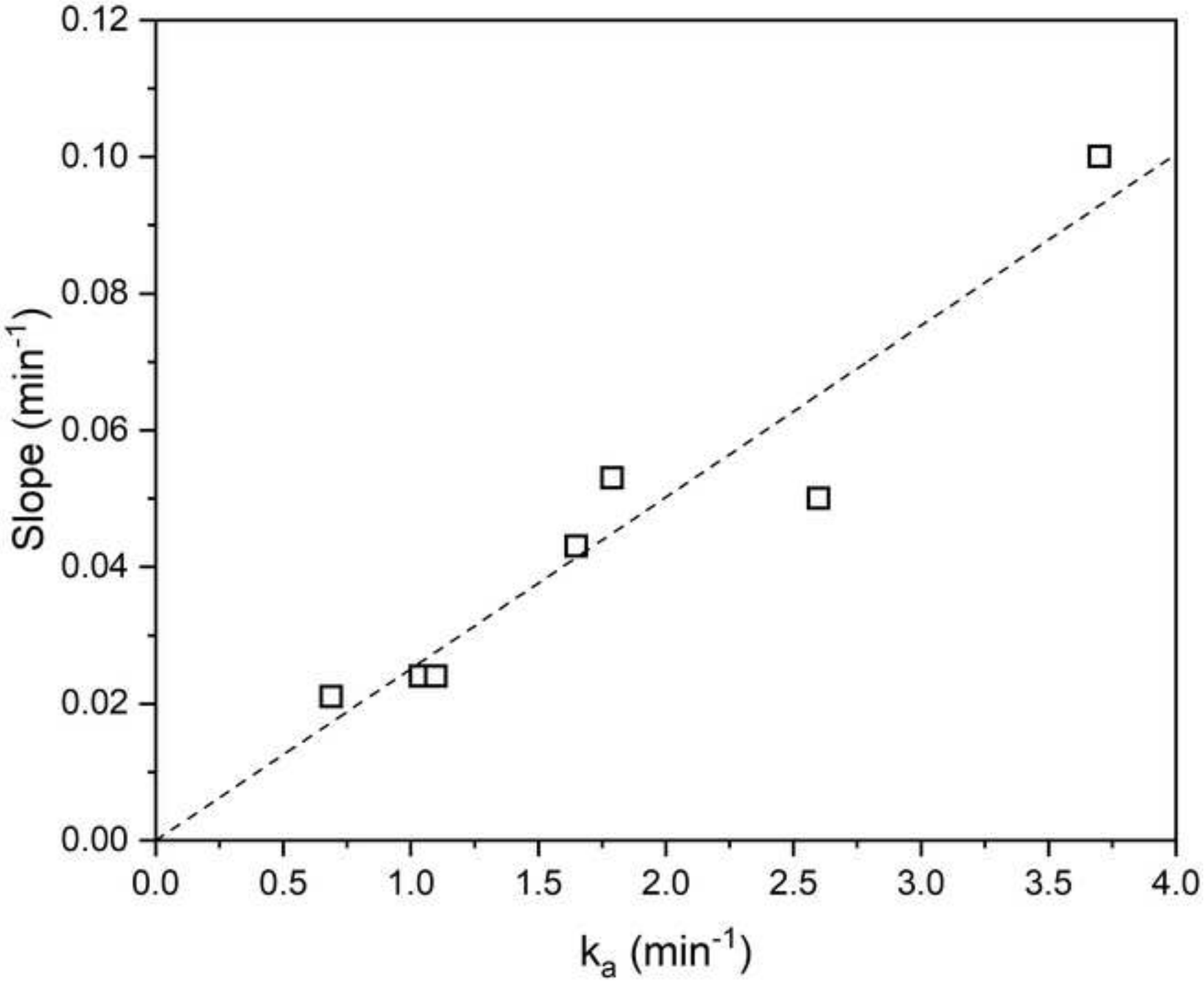

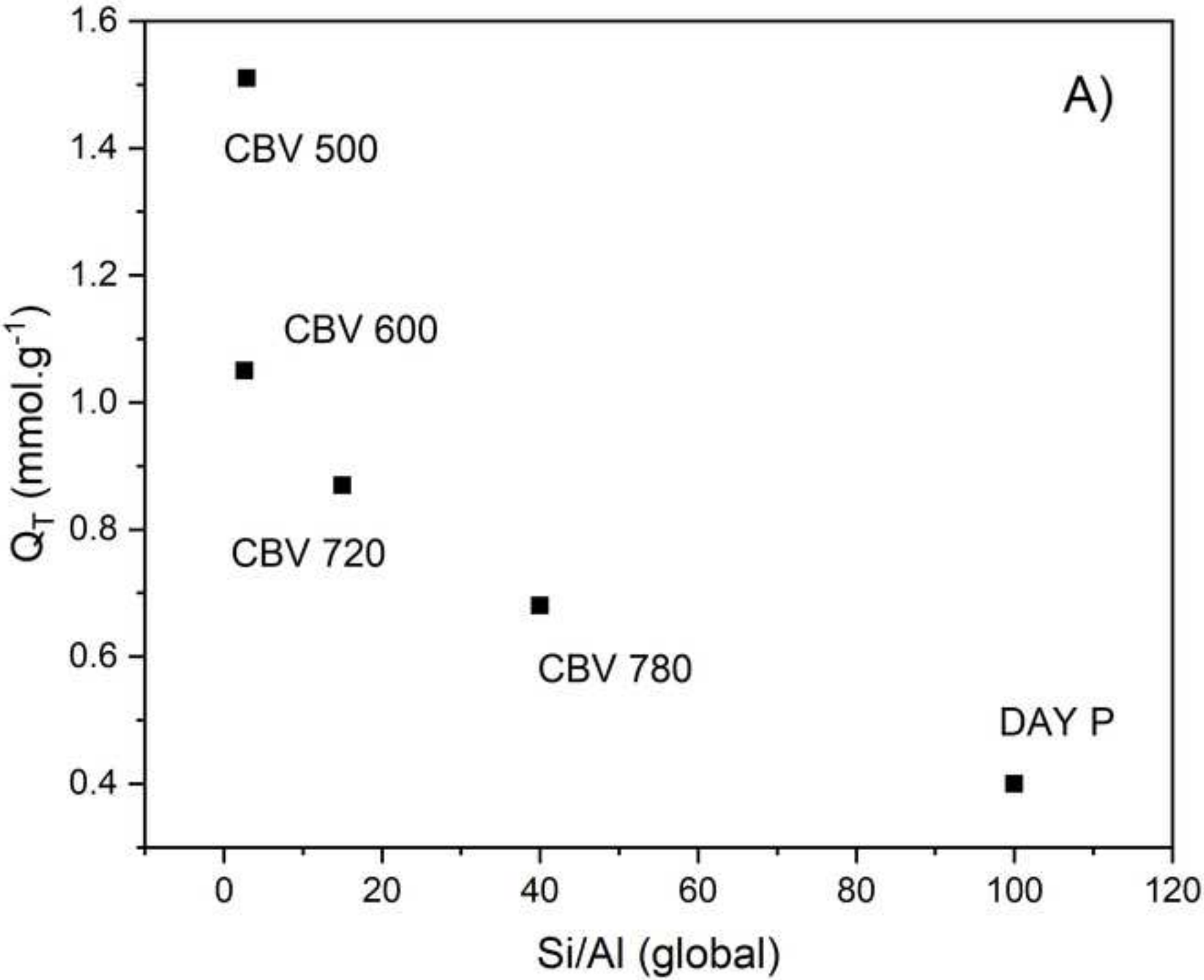

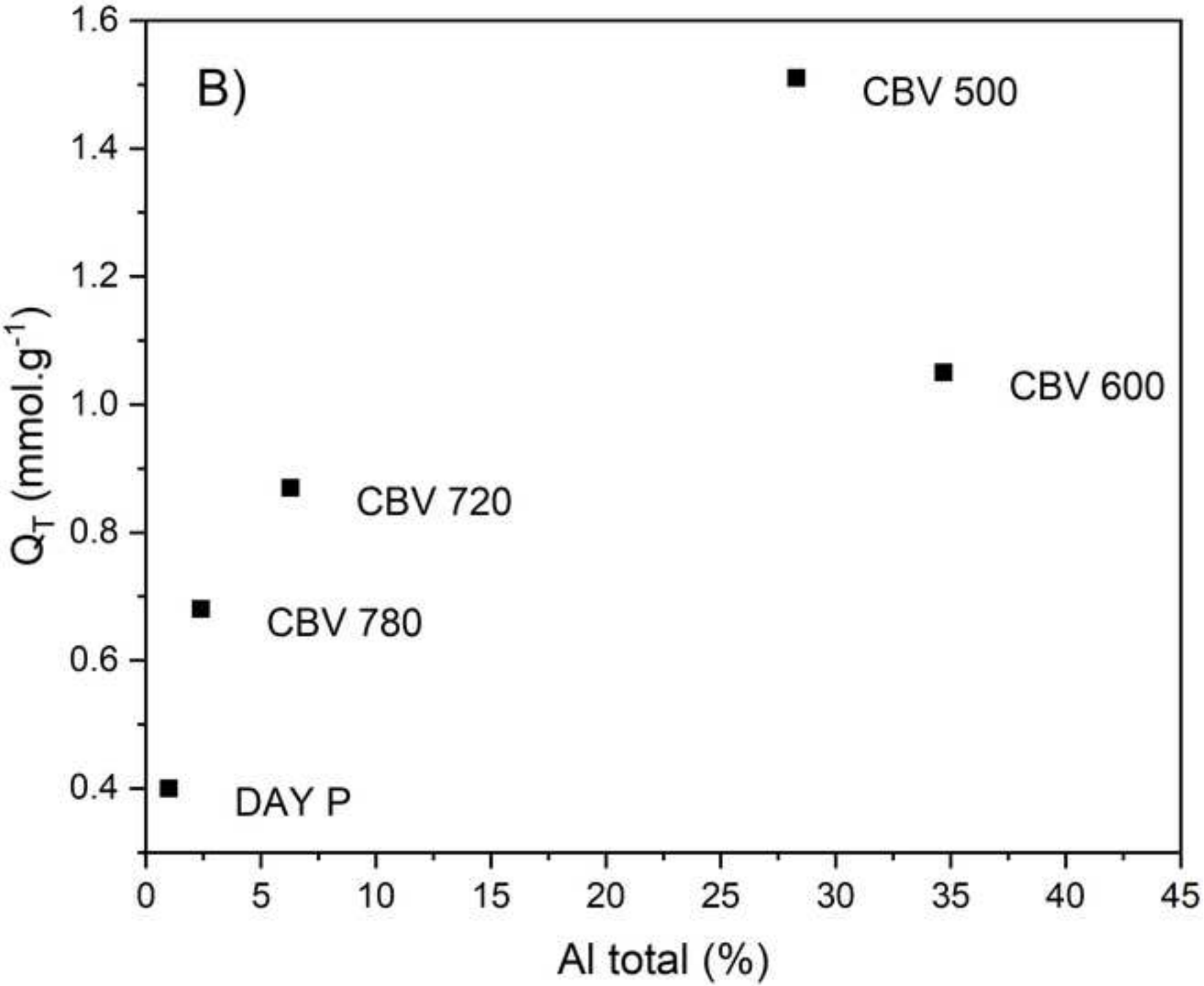

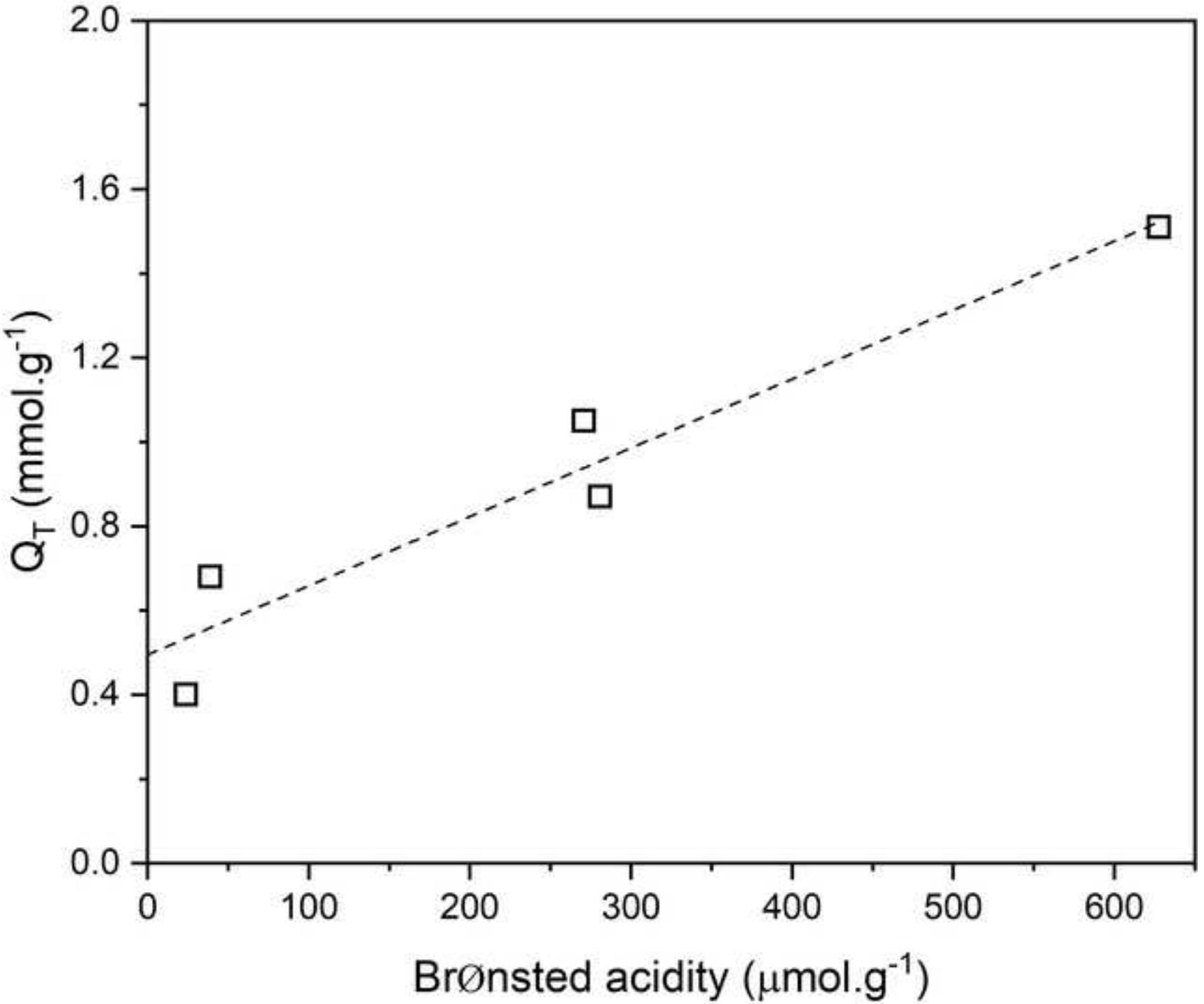

Fig8a

Click here to access/download;Figure(s);Fig8a AF-MMM-2021.jpg

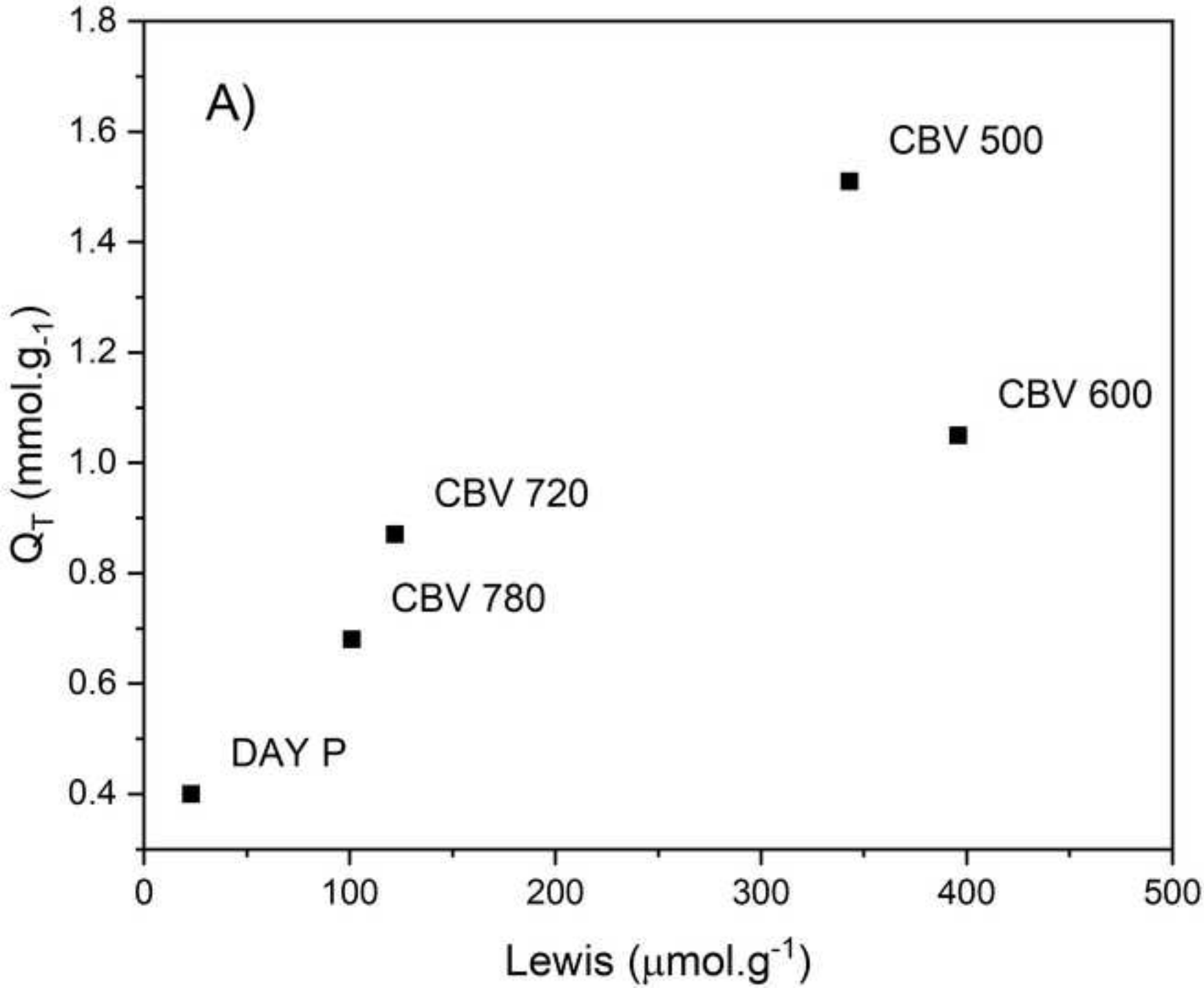

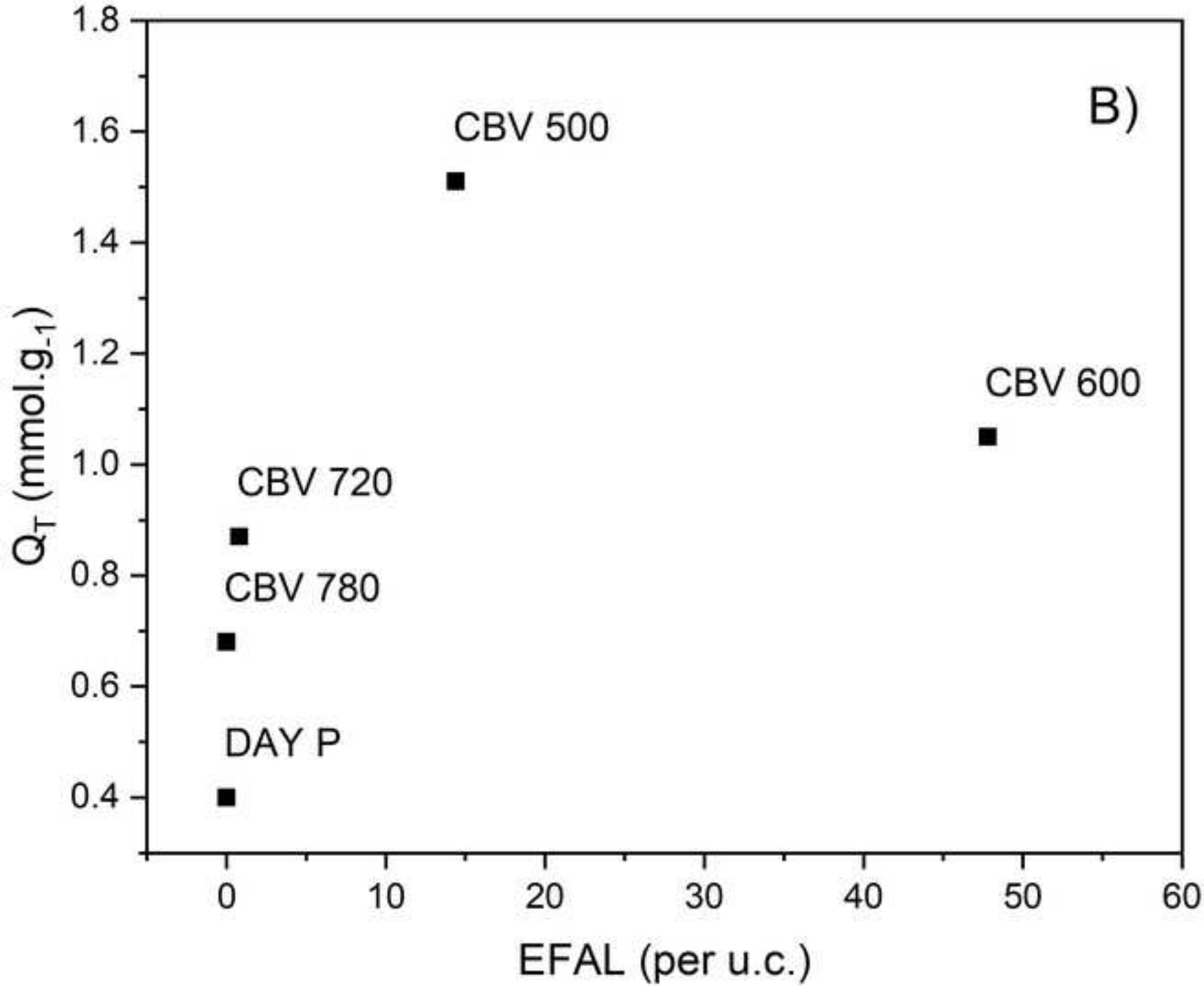

Fig9

Click here to access/download;Figure(s);Fig9 AF-MMM-2021.jpg

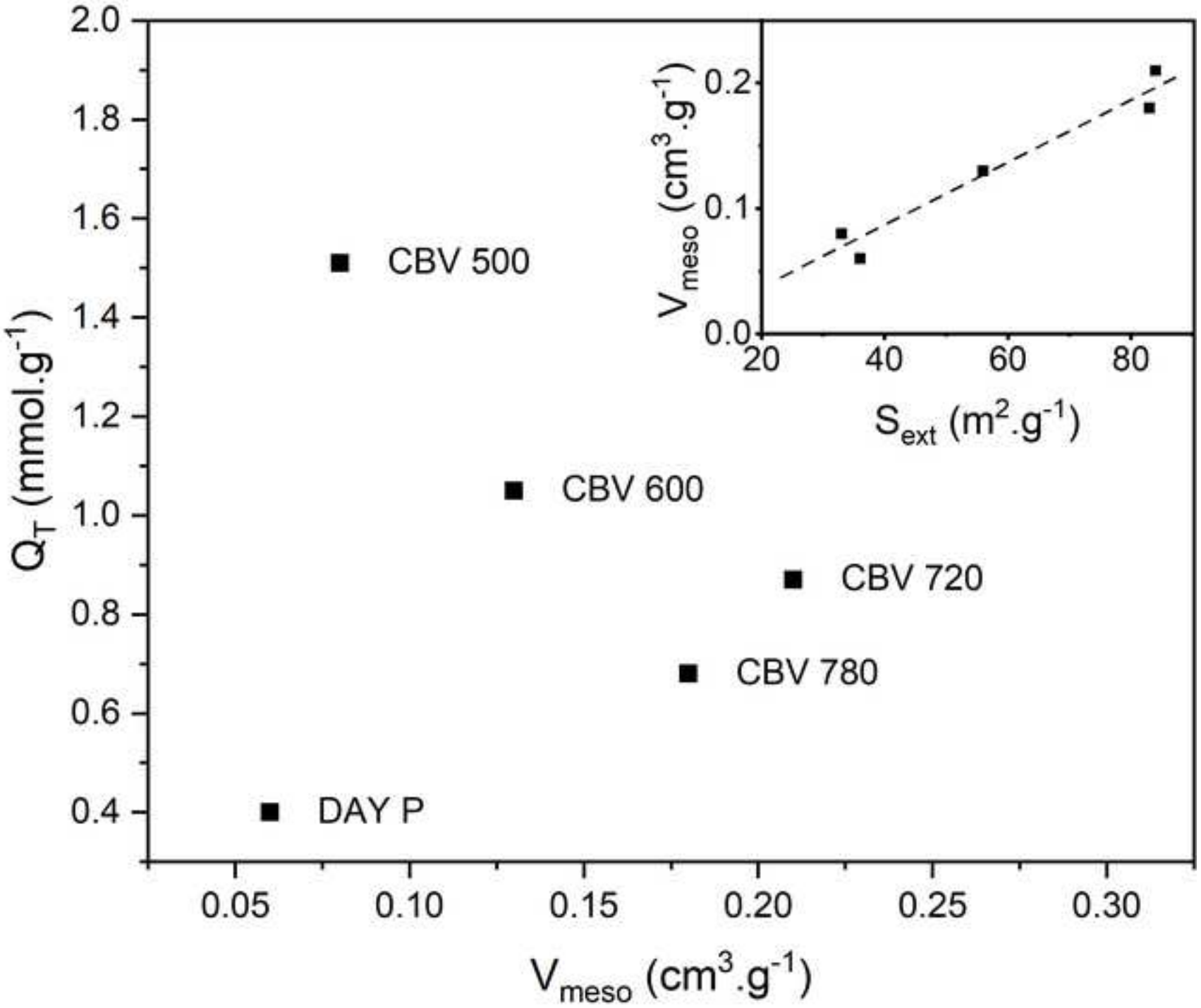

Credit authors statement

João Miguel Silva: Conceptualization, Methodology, Validation, Formal analysis, Software, Writing - review & editing. **Filipa Ribeiro**: Conceptualization, Methodology, Writing - review & editing, Funding acquisition, Project administration**. Inês Graça**: Conceptualization, Methodology, Investigation, Validation, Writing - original draft and review & editing. **Auguste Fernandes**: Conceptualization, Methodology, Investigation, Validation Writing - original draft and review & editing.

Declaration of interests

☒ The authors declare that they have no known competing financial interests or personal relationships that could have appeared to influence the work reported in this paper.

☐The authors declare the following financial interests/personal relationships which may be considered as potential competing interests:

Bio-oils/FCC co-processing: Insights into the adsorption of guaiacol on Y zeolites with distinct acidity and textural properties

J. M. Silva[a,b], M. F. Ribeiro[a], I. Graça[c*], A. Fernandes[a*]

[a]Centro de Química Estrutural and Departamento de Engenharia Química, Instituto Superior Técnico, Universidade de Lisboa, Av. Rovisco Pais, P-1049-001 Lisboa, Portugal
[b]Área Departamental de Engenharia Química, Instituto Superior de Engenharia de Lisboa, Instituto Politécnico de Lisboa, Rua Conselheiro Emídio Navarro, 1, 1959-007 Lisboa, Portugal
[c]University of Aberdeen, School of Engineering, Fraser Noble Building, King's College, Aberdeen AB24 3UE, Scotland, United Kingdom

[*]**Corresponding authors:** Auguste Fernandes, auguste.fernandes@tecnico.ulisboa.pt, phone: (+351) 218419183/fax: (+351) 218419198; Inês Graça, i.graca@abdn.ac.uk, phone: (+44) (0)1224 273293

Abstract

The guaiacol adsorption capacity of several Y zeolites with different physicochemical properties was tested by performing breakthrough adsorption experiments, in order to investigate the guaiacol adsorption on Fluid Catalytic Cracking catalysts during bio-oils/FCC feedstocks co-processing. X-Ray diffraction, nitrogen sorption measurements and pyridine adsorption followed by Infrared Spectroscopy were used to determine the framework Si/Al ratio, the textural parameters, and finally the nature and amount of acid sites. Klinkenberg model was used to fit the experimental data and to obtain the guaiacol adsorption capacity and k_a (overall coefficient of mass transfer) and K_e (adsorption equilibrium constant) parameters, which are directly related to, respectively, kinetic and thermodynamic aspects. K_e values, and so guaiacol adsorption, were observed to increase with the total number of Brønsted and Lewis acid sites on the zeolites, as well as with the amount of Na exchange. Conversely, mesoporosity increases the diffusion rate of guaiacol inside the zeolite structure, leading to higher k_a values and decreasing guaiacol retention. Overall, data show that guaiacol adsorption on the FCC catalysts, and so its impact on the activity, might decrease with the catalyst age, owing to the changes on the FCC catalyst properties taking place during operation.

Keywords: Faujasite, guaiacol, adsorption, acidity, bio-oils co-processing

1. Introduction

In order to reduce the dependence on crude oil and decrease CO_2 emissions, traditional fossil fuels must be replaced by alternative fuels based on renewable sources, such as lignocellulosic biomass. Lignocellulosic biomass is currently one of the renewable sources of carbon that can be converted into liquids (bio-oils) able to be used as transportation fuels [1,2]. Furthermore, contrarily to petroleum, biomass presents the advantage of containing negligible amounts of sulphur, nitrogen and metals, and its balance of CO_2 is neutral. However, these wood-derived bio-oil fractions contain important amounts (up to 45 wt.%) of oxygenated compounds, such as carboxylic acids, aldehydes, alcohols, ketones, esters, ethers, phenols, furans and carbohydrates. The presence of significant amounts of oxygenated molecules in the bio-oils composition gives them some undesirable properties, such as high viscosity, thermal and chemical instability, lower miscibility with hydrocarbons and high tendency to form coke [3–5].

The co-processing of bio-oils with conventional Fluid Catalytic Cracking (FCC) feedstocks could be a promising short-term possibility to produce bio-fuels [6,7]. However, the high amounts of O-compounds in the bio-oils can limit their direct addition to the FCC petroleum-based feedstocks. Hence, a previous upgrading of the bio-oils, by reducing their oxygen content, is normally required and can be performed by hydrodeoxygenation (HDO). Nevertheless, phenolic molecules are difficult to remove by HDO, and usually remain after the treatment [8–10].

The impact of lignin derived phenols, such as phenol and guaiacol, on FCC catalysts during bio-oils/FCC feedstocks co-processing has been explored in the literature. These oxygenates can have a detrimental impact on FCC catalysts. In fact, studies performed with the two main components of FCC catalyst, HY and HZSM-5 zeolites, revealed that phenolic molecules significantly and quickly deactivate these zeolites [2,11–14], due to the phenolic compounds adsorption on both Brønsted and Lewis acid sites, together with coke molecules. However, questions remain regarding how zeolite physicochemical properties can influence phenolic molecules adsorption. This is especially important considering that FCC catalysts are a mixture with a distribution of ages and chemical and physical properties, and phenolic

compounds adsorption. Therefore, their impact on activity might change depending on the age of the catalyst particles [15].

Some works related to adsorption of phenol [16–18] and phenolic compounds such as ortho-nitrophenol, para-nitrophenol, meta-nitrophenol, and 2,4-dinitrophenol on synthetic zeolites have been published. It was found that, for the FAU structure, the capacity of adsorption increased with the Si/Al ratio, and that, for the same Si/Al ratio, Y zeolite was more effective than BEA and mordenite [18,19]. However, so far, it appears that no data are available concerning guaiacol adsorption on synthetic zeolites.

Therefore, in this work, guaiacol adsorption was studied over several Y zeolites presenting very distinct physicochemical properties, by performing breakthrough adsorption experiments, to analyze the potential for guaiacol to adsorb on the FCC catalyst during bio-oils/FCC feedstocks co-processing. The breakthrough adsorption experiments were carried out in order to: a) analyze the diffusion ability of guaiacol molecules within the zeolite porous structures, b) evaluate the strength of the interaction between the zeolites and the O-compound, and c) determine the maximum amount of guaiacol that can be retained on the zeolites, under the experimental conditions selected. The influence of the Si/Al ratio, the presence of extra-framework aluminium (EFAL) species and sodium, and the textural properties on the adsorption process were evaluated. Finally, the conclusions obtained from the experimental data were extrapolated to the conditions of the bio-oils/FCC feedstocks co-processing.

2. Experimental

2.1. Materials

Different commercial Y zeolites (FAU structure), namely DAY P (Degussa), $Na_{2.1}$USHY (Grace Davison), CBV 720, CBV 780, CBV 600, CBV 500 (all from Zeolyst), were used as adsorbents. CBV 500 sample, supplied in the ammonium form, was calcined at 500 ºC under a flux of dry air to be converted into its protonic form. Besides these commercial Y zeolites, another zeolite sample was prepared from the $Na_{2.1}$USHY zeolite by increasing its Na content. For that purpose, an ammonium form of this zeolite was firstly prepared by subjecting the zeolite to a three-time ion-exchange treatment under reflux with a 2 M ammonium nitrate aqueous solution, at 100 ºC, for 4 h, using a solution/zeolite ratio of 4 mL g^{-1}. After ion-exchange, the suspension was filtered under vacuum and the zeolite obtained was

washed with deionized water and dried overnight in an oven at 100 ºC. Then, a 4 h ion-exchange was performed (three times) at room temperature, with a solution/zeolite ratio of 4 $mL.g^{-1}$, by using a 2 M sodium nitrate aqueous solution. Finally, the zeolite sample obtained after Na-exchange was filtered under vacuum, dried overnight in an oven at 100 ºC and calcined at 500 ºC under a flux of dry air (referred to as $Na_{3.0}$USHY).

2.2. Characterization

Powder X-Ray diffraction (PXRD) patterns were recorded on a Bruker AXS Advance D8 diffractometer. Powder patterns were taken at room temperature between 5 and 40 º (2θ), with a scan step of 0.02 º and a time step of 6 s, using Cu-Kα radiation. NaCl was used as an internal standard and mixed with the samples. The unit cell parameter a_o was subsequently calculated from each diffractogram, using CELREF software and Si/Al ratio obtained using the empirical formula from [20].

Elemental chemical analyses were performed by inductively coupled plasma atomic emission spectrometry (ICP-AES), using a Philips ICP PU 7000 spectrometer, after acid digestion of the samples.

Particle size distribution curves of the zeolite samples were determined by Laser diffraction, using a CILAS 1064 particles size analyzer from Malvern.

Nitrogen adsorption measurements were carried out at -196 °C on a Micrometrics ASAP 2010 apparatus. Before adsorption, the fresh zeolite samples were degassed under vacuum at 90 °C for 1 h and then at 350 °C for at least 4 h. N_2 isotherms were used to determine the total porous volume (V_{total}), the micropores volume (V_{micro}), the external surface area (S_{ext}) and the pores size distribution (PSD) curves. The total pore volume was calculated from the adsorbed volume of nitrogen for a relative pressure P/P_0 of 0.97, whereas V_{micro} and S_{ext} were determined using the *t*-plot method. The mesopores volume (V_{meso}) was given by the difference V_{total} - V_{micro}. The PSD curves were calculated from the analysis of the isotherm adsorption branch based on the Barrett-Joyner-Halenda (BJH) algorithm.

The samples acidity was characterized by pyridine adsorption followed by FTIR spectroscopy, using a Nicolet Nexus spectrometer. The samples were pressed into thin wafers (10-20 mg cm^{-2}) and pre-treated in an IR quartz cell at 450 ºC for 2 h under secondary vacuum (10^{-6} mbar). The samples were then cooled down to 150 ºC and contacted with pyridine (P_{eq} = 1.5 mbar) during 10 min. Then, pyridine excess was removed for 30 min under secondary

vacuum and the IR spectra were recorded. The concentrations of Brønsted and Lewis sites able to retain the pyridine at 150 ºC were determined using the integrated areas of the bands at 1545 and 1455 cm^{-1}, respectively, and using extinction coefficients from literature [21].

The determination of theoretical adsorption energies for guaiacol on the Brønsted and Lewis acid sites of the zeolites, as well on the basic Si-ONa-Al sites, were estimated based on density functional theory (DFT) calculations, using the molecular modelling software Spartan v1.1.0. The Brønsted and Lewis acid sites were represented by simple clusters with formulas $AlSiOH_7$ and $AlSi_3O_3H_9$, respectively. For the Si-ONa-Al sites, a $AlSiONaH_6$ cluster was used. The hybrid B3LYP functional formalism and the 6-31G* atomic orbital basis set were employed to optimize the zeolite clusters, guaiacol geometry and cluster + adsorbed molecule configurations. The theoretical adsorption energies were calculated as $\Delta E_{adsorption}$ = E (cluster+adsorbed molecule) - E (cluster) - E (molecule gaseous phase).

2.3. Breakthrough adsorption experiments

The breakthrough adsorption experiments were carried out in a vertical Pyrex fixed-bed column at 150 °C, under atmospheric pressure, in the gas phase. Before each adsorption experiment, the zeolites were pre-treated at 200 °C under dry air flow (60 $mL.min^{-1}$) for 1 h and cooled down to the adsorption test temperature.

To keep the length of the zeolite bed constant (1.5 cm) around 120 mg of each zeolite were used. The feed was constituted by a solution of 1.2 wt.% of guaiacol (Sigma-Aldrich, 99%) in *n*-heptane (Sigma-Aldrich, 99%) and N_2, with a N_2/guaiacol mixture molar ratio of 9. N_2 was added to decrease the partial pressure of the guaiacol mixture and allows for its complete vaporization at the breakthrough adsorption experiment temperature. The mixture flow rate (3 $mL.h^{-1}$) was kept constant with a B|Braun compact perfusor. Variation of guaiacol vapor concentration during the adsorption experiments was monitored with a Chrompack CP 9001 gas chromatograph. The chromatographic column was a Varian CP SIL 5CB fused silica column with a dimethylpolysiloxane stationary phase and following dimensions: 10 m x 0.32 mm i.d., 0.25 µm film thickness. The operating conditions were as follows: an injector temperature of 275 ºC; a detector temperature of 260 ºC; N_2 was the make-up gas (27 mL min^{-1}) and the oven temperature program was 5 min at 50 ºC.

The breakthrough adsorption curve is usually expressed in terms of the outlet/inlet concentrations ratio ($C(t)/C_0$) as a function of the operation time (t). The model of Klinkenberg

[22–24], Eq. 1, was used to fit the guaiacol adsorption breakthrough curves obtained experimentally.

$$\frac{C}{C_0} = \frac{1}{2}\left[1 + \text{erf}\left(\sqrt{\tau} - \sqrt{\xi} + \frac{1}{8\sqrt{\tau}} + \frac{1}{8\sqrt{\xi}}\right)\right] \quad \text{Eq. 1}$$

with $\text{erf}(x) = \frac{2}{\sqrt{\pi}}\int_0^x e^{-t^2}dt$; $\tau = k_a\left(t - \frac{z}{u}\right)$; $\xi = k_a K_e \frac{z}{u}\left(\frac{1-\varepsilon}{\varepsilon}\right)$

and where erf(x) is the error function, k_a the overall mass transfer coefficient, K_e the adsorption equilibrium constant, z the bed height, u the gas velocity, t the time and ε the bed void fraction. The following parameters were considered: ε = 0.3; z = 1.5 cm and u = 728 cm min^{-1}. The model was adjusted to the experimental data by minimizing the sum of the squared absolute errors for C/C_0. Based on this, k_a and K_e values were determined for each zeolite. The maximum adsorption capacity of the zeolites for guaiacol, Q_T (mmol g^{-1}), was also estimated from the model fitted curves, according to Eq. 2.

$$Q_T = \frac{\left(\int_0^{t_{saturation}} 1dt - \int_{t_{breakthrough}}^{t_{saturation}} \frac{C(t)}{C_0}dt\right) \times F_0}{m}, \quad \text{Eq. 2}$$

where breakthrough time ($t_{breakthrough}$) corresponds to the initial detection of the adsorbate at the adsorber outlet, i.e. the minimum time required to cross the adsorbent bed, saturation time ($t_{saturation}$) is the point when the maximum capacity of retention of the adsorbent is reached, F_0 the entry molar flux of guaiacol and m the mass of zeolite used. However, $t_{breakthrough}$ and $t_{saturation}$ times were replaced by $t_{5\%}$ and $t_{95\%}$ times (times required to desorb 5 and 95 % of the adsorbate respectively; also calculated from the model fitting), since these later parameters are normally preferred as they are more reliable. Finally, the breakthrough adsorption slope was determined for each zeolite, by considering a linear adjustment $C(t)/C_0$ versus time within the interval $t_{5\%}$ and $t_{95\%}$.

3. Results and discussion

3.1. Characterization

The main physicochemical characteristics of the different adsorbents used in this study are reported in Table 1. All the samples are well crystalline materials with a FAU structure. The framework Si/Al_{IV} ratio calculated for each sample from the PXRD patterns are reported in Table 1, together with the unit cell formula (obtained from chemical analysis and PXRD results), the Na content, the global Si/Al and the particles size. The accuracy of the framework Si/Al_{IV} determined by PXRD was corroborated by comparing the values obtained with framework Si/Al_{IV} from ^{29}Si NMR found in the literature for the same commercial Y zeolites [25]. The amount of EFAL (extra framework Al) species per unit cell was obtained by the difference of the total Al content (from global Si/Al ratio) and the framework Al content (framework Si/Al_{IV} ratio). Hydrogen content was then calculated to balance negative charges (together with Na species), in order to obtain a neutral unit cell formula. From the Table 1, it can be seen that the samples present a very large range of global Si/Al (2.6-100), framework Si/Al_{IV} ratio (3.7-40), EFAL species contents (0-47.8) and different Na content.

TABLE 1

Nitrogen isotherms and PSD curves obtained for all the samples are shown in Figure 1 (all the isotherms have been shifted vertically for sake of clarity). Table 2 gives the corresponding textural parameters, namely pore sizes (in the mesopores region), external surface area S_{ext} and pores volume (V_{micro} and V_{meso}). Basically, two groups of FAU zeolites can be distinguished: one group corresponding to samples essentially microporous (isotherm of type I with a horizontal plateau at high relative p/p_0), with no or very weak mesopores contribution, and another group corresponding to microporous materials with an important contribution of mesopores (isotherms I with a hysteresis loop at high p/p_0). Logically, the first group, consisting of $Na_{2.1}$USHY, $Na_{3.0}$USHY, CBV 500 and DAY P (see Figure 1, open symbols), presents low external surface area (S_{ext}< 40 m^2 g^{-1}) and small mesopores volume (V_{meso}< 0.10 cm^3 g^{-1}).

FIGURE 1

On the other hand, the second group containing the remaining samples (CBV 720, CBV 780 and CBV 600, Figure 1, closed symbols), shows higher external surface area (> 55 m^2 g^{-1}) and larger mesopores volume (> 0.13 cm^3 g^{-1}). The presence of substantial mesoporosity in the later samples could be attributed to the fact that those materials had been all subjected to a dealumination process (in order to increase the framework Si/Al_{IV} ratio), as they present a rather high value (> 5) when compared with the less dealuminated samples (Si/Al_{IV} < 5). Interestingly, DAY P sample, which is a highly dealuminated sample, does not present any significant mesoporosity. Additionally, all the samples show micropores volume values in the range 0.24-0.34 cm^3 g^{-1}, typical for this type of materials. Moreover, while free EFAL species samples present relatively high micropores volumes (0.30-0.33 cm^3 g^{-1}), the presence of EFAL species in the other samples slightly decreases the micropores volume (0.24-0.29 cm^3 g^{-1}). This effect is more pronounced for CBV 600 sample, which is the one presenting the highest EFAL species content (0.24 cm^3 g^{-1} for 47.8 EFAL species per unit cell).

TABLE 2

Table 2 also shows the quantitative results obtained from pyridine adsorption, namely the amount of both Brønsted (B) and Lewis (L) acid sites able to retain pyridine molecule at 150 ºC under vacuum. In Figure 2, the amount of total, Brønsted and Lewis acid sites as a function of, respectively, global Si/Al, framework Si/Al_{IV} and the amount of EFAL species per unit cell, is shown. The total acidity (B+L) naturally follows the global Si/Al ratio of the different samples (see Figure 2-A), i.e., the higher the global Si/Al ratio, the lower the total acidity. The following total acidity amount order was observed: DAY P (Si/Al = 100) << CBV 780 (40) << CBV 720 (15) < CBV 600 (2.6), $Na_{2.1}$USHY (2.8), $Na_{3.0}$USHY (2.8) < CBV 500 (2.9).

On the other hand, Brønsted acidity can also be directly correlated with the framework Si/Al_{IV} ratio, as it can be seen in Figure 2-A. DAY P and CBV 780 are the materials that present the highest Si/Al_{IV} ratios (respectively 100 and 40) and logically present the lower amount of Brønsted sites, respectively 24 and 39 μmol g^{-1}. $Na_{2.1}$USHY, $Na_{3.0}$USHY and CBV 500, with Si/Al_{IV} of about 3.7-4.0, have the highest amount of Brønsted acid sites, with the two first

having a slightly lower value because of the presence of compensating Na^+ cations. CBV 720 and CBV 600 present an intermediate Brønsted value, as their Si/Al_{IV} ratio is about 9-16.

FIGURE 2

Concerning Lewis acid sites, here again it can be seen that the amount of Lewis sites follows the amount of EFAL species in the unit cell (Figure 2-B). However, CBV 600 sample, with an amount of 47.8 EFAL per unit cell, does not have much more Lewis acid sites than, for example, CBV500 sample (14.4 EFAL). A possible explanation could be that some Lewis sites might not be accessible to pyridine molecules, probably because of some hindrance caused by the presence of a very large amount of EFAL species in this sample.

All the adsorbents used in this work have a FAU structure, which is usually accessible to aromatic molecules with relatively large kinetic diameters, owing to the presence of supercages characterized by 12-membered rings (12-MR) with an open diameter of 7.4 Å. Through DFT calculations using the software Spartan, a kinetic diameter of 6.6 Å was estimated for guaiacol, which might indicate that the adsorption of guaiacol occurs preferentially on the supercages of the Y zeolites. In addition, it is also well-known that guaiacol interacts with both Brønsted and Lewis acid sites [14]. Theoretical adsorption energies calculated from Spartan software show that the interaction of guaiacol with Lewis acid sites (-108 kJ mol^{-1}) is stronger than with Brønsted acid sites (-88 kJ mol^{-1}). Interestingly, the theoretical adsorption energy of guaiacol on basic Na-exchanged zeolite framework sites was found to be -104 kJ mol^{-1}. Being similar to that estimated for Lewis acid sites, this might anticipate that Na presence also favors guaiacol adsorption.

3.2. Adsorption performance

Illustrative breakthrough curves, corresponding to the adsorption of 1.2 wt.% of guaiacol in *n*-heptane, obtained for DAY P and $Na_{2.1}$USHY samples, are presented in Figure 3. The results (amount of adsorbed guaiacol Q_T, breakthrough curves slopes, $t_{5\%}$ and $t_{95\%}$) extracted from the fitting curves are presented in Table 3, together with parameters k_a and K_e

also obtained from the model fit. The amount of guaiacol adsorbed by each sample was also confirmed by thermogravimetric measurements.

TABLE 3

FIGURE 3

Guaiacol breakthrough results show that all the samples reach a guaiacol adsorption equilibrium. However, from the different curves obtained, and also from the parameters extracted from the experimental fittings, one can distinguish once again two main groups. The first one (Group I) corresponds to samples DAY P (illustrated in Figure 3-A), CBV 720, CBV 780 and CBV 600 and is defined by the following features: small $t_{5\%}$ (< 30 min) and $t_{95\%}$ (< 50 min) and a very small difference between $t_{5\%}$ and $t_{95\%}$, demonstrated by a steep breakthrough curve slope ($\geq$ 0.043 min^{-1}, see Table 3). On the other hand, the second group (Group II), corresponding to samples CBV 500, $Na_{2.1}$USHY (illustrated in Figure 3-B) and $Na_{3.0}$USHY, can be defined by longer $t_{5\%}$ ($\geq$ 35 min) and $t_{95\%}$ ($\geq$ 77 min), resulting in a gentler breakthrough curve slope (< 0.025 min^{-1}). The direct consequence is the final guaiacol capacity that is very different from one group to the other: 1.05 mmol g^{-1} or less for the first group and 1.51 mmol g^{-1} or more for the second group.

Concerning the parameters k_a and K_e obtained from the Klinkenberg model, one can see that samples with a higher guaiacol adsorption capacity (Group II) have higher adsorption equilibrium constants ($K_e > 11x10^3$), while samples having a poorer guaiacol adsorption (Group I) present lower K_e values ($< 7x10^3$). Indeed, a very good linear correlation can be obtained by simply plotting the amount of guaiacol adsorbed, Q_T, as a function of K_e (see Figure 4), clearly showing that guaiacol adsorption onto FAU samples is essentially ruled by thermodynamics considerations. In the next section, it will be shown how FAU zeolites properties can explain this result. Concerning the overall coefficient of mass transfer (k_a), this

expresses how fast guaiacol molecules diffuse through the zeolite porous system. It can be seen in Table 3 that zeolites of Group I present higher k_a values (1.65-3.70 min^{-1}) than those belonging to Group II (0.69-1.10 min^{-1}). This means that diffusion of guaiacol is much faster on DAY P, CBV 720, CBV 780 and CBV 600 zeolites than on CBV 500, $Na_{2.1}$USHY and $Na_{3.0}$USHY zeolites, which correlates well with the slopes estimated for the breakthrough adsorption curves (Figure 5). Indeed, the lower the k_a value, the smoother the slope of the breakthrough curve, meaning a higher difference between $t_{5\%}$ and $t_{95\%}$. It is well known that molecules diffusion within the pores of a zeolite mainly takes place through the interaction with pore walls. Thus, the stronger the guaiacol adsorption to the pore walls of the zeolites, the lower the ability for the guaiacol molecules to diffuse through the zeolite porous system, which explains the lower k_a values (lower slopes values) for the zeolites of Group II.

FIGURE 4

FIGURE 5

3.3. Guaiacol adsorption vs zeolite properties

3.3.1. Sodium influence

With the purpose of studying the effect of the presence of sodium in zeolites framework on the guaiacol adsorption, zeolites $Na_{2.1}$USHY, $Na_{3.0}$USHY and CBV 500 were chosen, as they present similar physicochemical properties, except for the amount of Na. The two first zeolites are the only ones presenting Na in their framework as compensating cation, as it can be seen in Table 1. Na content on FCC catalysts can typically range from 0.2 to 0.5 wt.% upon exposure to the Na-containing FCC feedstocks. Considering the maximum value of 0.5 wt.% and the fact that the FCC catalysts usually contain 10-40 wt.% of Y zeolite in their formulations [15], the Na content on the pure zeolite can range from about 1 to 5 wt.%. Therefore, 2 and 3

wt.% of Na were chosen as representative amounts. It can be observed that presence of Na in the zeolite structure (up to 3 wt.%) seems to increase the guaiacol adsorption. This is not strange considering that the theoretical adsorption energy of guaiacol is higher on the basic Na-exchanged zeolite framework sites (-104 kJ mol^{-1}) than on the Brønsted acid sites (-88 kJ mol^{-1}). Indeed, Beutel *et al.* reported, by employing ^{1}H and ^{29}Si MAS NMR spectroscopy, that hydrogen bonding of phenol to the oxygen atoms of the zeolite is not the only interaction between phenol and Na-X zeolite. Of the same importance is the interaction of phenol aromatic ring with either Na^{+} cations or oxygens of zeolite supercages [26]. Some other studies also demonstrated similar phenol interaction with exchanged cations and zeolite oxygens [27,28].

3.3.2. Si/Al ratio influence

Zeolites, which are porous crystalline aluminosilicates, are formed by SiO_4 and AlO_4 tetrahedra connected by oxygen atoms, and their hydrophilic/hydrophobic character will depend essentially on the Si/Al framework ratio. It is generally accepted that for Si/Al < 10, zeolites are hydrophilic, i.e. water can interact easily with compensating cations (protons, etc.), while for Si/Al > 10, they turn hydrophobic because of the presence of non-polar ≡Si-O-Si≡ bridging groups [29]. Several studies have investigated the application of synthetic zeolites for the adsorption of phenolic compounds from wastewater and noticed the improvement of adsorption capacity with increased hydrophobicity [16,17,30,31]. In our case, the amount of guaiacol adsorbed onto the different FAU adsorbents as a function of Si/Al ratio and percentage of Al is illustrated in Figure 6. As it can be seen, the adsorption of guaiacol is favored using FAU zeolites with a low Si/Al ratio of about 4 (high number of aluminum atoms), i.e., zeolites with a rather hydrophilic character. This shows the importance of the number of framework and extra framework Al for the adsorption of guaiacol, in absence of an adsorption competition with water. Although this later condition is necessary, it is not enough to explain why CBV 600 sample is less efficient to adsorb guaiacol, although it has the same global Si/Al ratio as, for example, CBV 500 sample. This will be analyzed later in this paper.

FIGURE 6

3.3.3. Acid sites and EFAL species

From Figure 6 (B), one could see that the amount of Al in the zeolites plays a crucial role in the adsorption of guaiacol. Normally, zeolites present two types of Al species: Al species that are incorporated on the zeolite framework and account for the Brønsted acidity, and extra framework Al species. These extra framework (EFAL) Al species (octahedral, oligomers species or tri-coordinated Al) present in FAU structures are known to be responsible for the Lewis acidity of zeolites. Therefore, if guaiacol adsorption generally increases with the total number of Al, this is the same as saying that a higher guaiacol retention is expected for samples with a higher total amount of Brønsted and Lewis acid sites, which is indeed observed in Table 3. Following our findings concerning the estimated theoretical adsorption energies, it seems reasonable that both Brønsted and Lewis acid sites are responsible for the adsorption of guaiacol on the different FAU adsorbents. In fact, when plotting the evolution of the amount of guaiacol adsorbed as a function of the number of Brønsted acid sites (Figure 7), an increase in the amount of guaiacol retained on the zeolites can be seen with the Brønsted acidity. Figure 8 shows the amount of guaiacol adsorbed as a function of Lewis acidity (A) and EFAL species (B). Indeed, it also seems that guaiacol adsorption capacity follows both the Lewis acidity and EFAL amounts. However, in this latter case, the guaiacol adsorption passes through a maximum for CBV 500 sample, which is followed by a decrease for CBV 600. This result is unexpected considering that CBV 600 zeolite is the sample presenting the highest amount of EFAL species or Lewis acid sites, which were observed by DFT calculations to have a higher adsorption energy for guaiacol. The behavior of CBV 600 sample can be easily explained, taking into account the accessibility of the acid sites to the guaiacol molecules, which might be partially hindered by the large amount of EFAL species present in this sample. This conclusion is also supported by the previous observation on the underestimation of the Lewis acid sites by pyridine adsorption.

FIGURE 7

FIGURE 8

3.3.4. Textural parameters influence

Figure 9 shows the amount of guaiacol adsorbed (Q_T) on the various zeolites as a function of the mesoporous volume (V_{meso}), together with the linear relationship between V_{meso} and external surface area S_{ext}. When all the samples are compared, with exception of DAY P, the zeolites with a relatively high V_{meso} (> 0.10 $cm^3\ g^{-1}$) adsorb less guaiacol (< 1.10 mmol g^{-1}). This is quite surprising, considering that higher mesoporous volumes should lead to more space available to adsorb the bulky guaiacol molecules. Therefore, a higher guaiacol retention should be expected for the samples presenting an enhanced mesoporous volume. However, it is also known that the presence of mesopores in combination with micropores in zeolites is responsible for an increase in the diffusion rate of the guaiacol molecules inside the zeolite structure [2]. Indeed, according to the breakthrough curves slopes and k_a in Table 3, samples presenting improved mesoporous volume and external surface area are those for which a sharp slope and higher k_a values (higher diffusion rates) were found. Therefore, the increase in the diffusion rate generated by the higher mesoporous volume seems to prevail over the increase in space, in what concerns the guaiacol adsorption on the zeolites. In the case of the microporous volume, this one is generally similar for all the zeolite samples, except for CBV600 which presents a lower microporous volume. As previously mentioned, the high number of EFAL species on this sample might partially block its porous structure, decreasing the micropores volume, the accessibility to the acid sites and, consequently, reducing the guaiacol adsorption.

FIGURE 9

Overall, these results demonstrate that for acidic zeolites the total number of Brønsted and Lewis acid sites is the most important parameter that governs the amount of guaiacol adsorbed. Nevertheless, the presence of mesoporosity also seems to have an impact on the

guaiacol adsorption, as it increases the diffusion rate of guaiacol molecules. In addition, adsorption of guaiacol is increased if protons are exchanged by Na as compensating cations. Considering the properties of the catalyst used in the FCC process, these results can be extrapolated to the conditions of the bio-oils/FCC feedstocks co-processing. The equilibrium catalyst circulating in the FCC unit is composed by a mixture of catalyst particles with different ages and different chemical and textural properties [15]. Typically, the fresh ultra-stable Y (USY) zeolite used in the process has a low Si/Al framework ratio of 5. However, even though this USY catalyst is produced by controlled dealumination and presents an increased hydrothermal stability, it still undergoes further dealumination when submitted to the consecutive regeneration steps [32,33]. As a result, Al atoms are released from the zeolite framework, leading to an increase in the Si/Al framework ratio to 5-20. Consequently, this causes a reduction in the number of Brønsted acid sites, an increase in the Lewis acid sites (as EFAL species are generated) and an increase in the mesoporous volume of the zeolite. Therefore, adsorption of guaiacol is expected to be higher on fresh FCC catalyst, due to lower Si/Al ratio, higher amount of Brønsted acid sites and moderate quantity of EFAL species. On the other hand, an aged FCC catalyst with a higher Si/Al, a lower number of Brønsted acid sites and a higher number of EFAL species (that may hinder adsorption as observed) should adsorb a lower number of guaiacol molecules during co-processing. Additionally, the higher mesopores volume of the aged FCC catalyst would also facilitate the diffusion of the guaiacol molecules, decreasing their retention inside the zeolite structure. On the other hand, it is also known that Na content on the FCC catalysts also increases with circulation time, due to the presence of Na-containing compounds in the feed [15]. As observed, this increase in the sodium content should increase the amount of guaiacol adsorbed. However, Na passivators are used on the FCC catalyst to avoid the protons being exchanged by the Na, which would minimize this effect. Thus, the different guaiacol adsorption capacities for the fresh and aged FCC catalysts would certainly have implications on the poisoning effect of guaiacol during bio-oils/FCC feedstocks co-processing. Given the expected higher retention of guaiacol on the fresh FCC catalyst, a higher detrimental effect should be anticipated in this case.

4. Conclusions

Various FAU zeolites, with different framework Si/Al ratios (ranging from 3 to 100), amounts of Brønsted and Lewis acid sites and textural parameters, were tested for the adsorption of guaiacol. The parameters obtained from experimental guaiacol adsorption breakthrough curves and subsequent model fitting, i.e. guaiacol capacity, adsorption equilibrium constant (K_e), coefficient of mass transfer (k_a), $t_{5\%}$ and $t_{95\%}$, breakthrough curve slopes showed a direct correlation with the physicochemical properties of the zeolites. All the results show that materials with low Si/Al ratio (about 4) and high total amount of both Brønsted and Lewis acid sites (> 600 μmol g^{-1}) present a higher guaiacol adsorption, as well as higher K_e values, confirming theoretical adsorption energies calculations. On the other hand, zeolites with higher mesoporous volumes or external surface area led to a higher diffusion rate within the zeolite structure (higher k_a values), decreasing guaiacol retention. In addition, the replacement of protons by sodium atoms as compensating cations was also observed to increase guaiacol adsorption. Taking into account the changes that take place on the FCC catalyst properties during operation, it is expected that the poisoning effect of guaiacol during bio-oils/FCC feedstocks co-processing is attenuated with the increase of the catalyst age.

Acknowledgments

The authors thank Fundação para a Ciência e a Tecnologia (FCT, Portugal) for financial funding (UIDB/00100/2020 and UIDP/00100/2020). Fernandes also thanks FCT for researcher contract hiring (DL No. 57/2016 regulation).

References

[1] S.-Y. No, Application of bio-oils from lignocellulosic biomass to transportation, heat and power generation - A review, Renew. Sustain. Energy Rev. 40 (2014) 1108–1125. https://doi.org/http://dx.doi.org/10.1016/j.rser.2014.07.127.

[2] I. Graça, A.M. Carmo, J.M. Lopes, M.F. Ribeiro, Improving HZSM-5 resistance to phenolic compounds for the bio-oils/FCC feedstocks co-processing, Fuel. 140 (2015) 484–494. https://doi.org/http://dx.doi.org/10.1016/j.fuel.2014.10.002.

[3] Q. Lu, W.-Z. Li, X.-F. Zhu, Overview of fuel properties of biomass fast pyrolysis oils, Energy Convers. Manag. 50 (2009) 1376–1383.

https://doi.org/http://dx.doi.org/10.1016/j.enconman.2009.01.001.

[4] M. Badawi, J.-F. Paul, S. Cristol, E. Payen, Guaiacol derivatives and inhibiting species adsorption over MoS2 and CoMoS catalysts under HDO conditions: A DFT study, Catal. Commun. 12 (2011) 901–905. https://doi.org/http://dx.doi.org/10.1016/j.catcom.2011.02.010.

[5] J.D. Martínez, A. Veses, A.M. Mastral, R. Murillo, M. V Navarro, N. Puy, A. Artigues, J. Bartrolí, T. García, Co-pyrolysis of biomass with waste tyres: Upgrading of liquid bio-fuel, Fuel Process. Technol. 119 (2014) 263–271. https://doi.org/http://dx.doi.org/10.1016/j.fuproc.2013.11.015.

[6] I. Graça, J.M. Lopes, H.S. Cerqueira, M.F. Ribeiro, Bio-oils Upgrading for Second Generation Biofuels, Ind. Eng. Chem. Res. 52 (2013) 275–287. https://doi.org/10.1021/ie301714x.

[7] S.D. Stefanidis, K.G. Kalogiannis, A.A. Lappas, Co-processing bio-oil in the refinery for drop-in biofuels via fluid catalytic cracking, WIREs Energy Environ. 7 (2018) e281. https://doi.org/https://doi.org/10.1002/wene.281.

[8] A. Centeno, E. Laurent, B. Delmon, Influence of the Support of CoMo Sulfide Catalysts and of the Addition of Potassium and Platinum on the Catalytic Performances for the Hydrodeoxygenation of Carbonyl, Carboxyl, and Guaiacol-Type Molecules, J. Catal. 154 (1995) 288–298. https://doi.org/http://dx.doi.org/10.1006/jcat.1995.1170.

[9] V.N. Bui, G. Toussaint, D. Laurenti, C. Mirodatos, C. Geantet, Co-processing of pyrolisis bio oils and gas oil for new generation of bio-fuels: Hydrodeoxygenation of guaïacol and SRGO mixed feed, Catal. Today. 143 (2009) 172–178. https://doi.org/http://dx.doi.org/10.1016/j.cattod.2008.11.024.

[10] E. Furimsky, Hydroprocessing challenges in biofuels production, Catal. Today. 217 (2013) 13–56. https://doi.org/http://dx.doi.org/10.1016/j.cattod.2012.11.008.

[11] I. Graça, J.M. Lopes, M.F. Ribeiro, M. Badawi, S. Laforge, P. Magnoux, F. Ramôa Ribeiro, n-Heptane cracking over mixtures of HY and HZSM-5 zeolites: Influence of the presence of phenol, Fuel. 94 (2012) 571–577. https://doi.org/http://dx.doi.org/10.1016/j.fuel.2011.11.033.

[12] I. Graça, A. Fernandes, J.M. Lopes, M.F. Ribeiro, S. Laforge, P. Magnoux, F. Ramôa Ribeiro, Effect of phenol adsorption on HY zeolite for n-heptane cracking: Comparison with methylcyclohexane, Appl. Catal. A Gen. 385 (2010) 178–189. http://internal-pdf//Applied Catalysis A General 385 (2010) 178–189-

3558158849/Applied Catalysis A General 385 (2010) 178–189.pdf.

[13] I. Graça, A. Fernandes, J.M. Lopes, M.F. Ribeiro, S. Laforge, P. Magnoux, F. Ramôa Ribeiro, Bio-oils and FCC feedstocks co-processing: Impact of phenolic molecules on FCC hydrocarbons transformation over MFI, Fuel. 90 (2011) 467–476. http://internal-pdf//Fuel 90 (2011) 467–476-1059295232/Fuel 90 (2011) 467–476.pdf.

[14] R.T.J. Gerards, A. Fernandes, I. Graça, M.F. Ribeiro, Towards understanding of phenolic compounds impact on Ni- and V-USY zeolites during bio-oils co-processing in FCC units, Fuel. 260 (2020) 116372. https://doi.org/https://doi.org/10.1016/j.fuel.2019.116372.

[15] R. Sadeghbeigi, Fluid Catalytic Cracking Handbook: Design, Operation and Troubleshooting of FCC Facilities, 2nd Ed., Gulf Professional Publishing, 2000.

[16] M. Ahmaruzzaman, Adsorption of phenolic compounds on low-cost adsorbents: A review, Adv. Colloid Interface Sci. 143 (2008) 48–67. https://doi.org/http://dx.doi.org/10.1016/j.cis.2008.07.002.

[17] L. Damjanovíc, V. Rakíc, V. Rac, D. Stosíc, A. Auroux, The investigation of phenol removal from aqueous solutions by zeolites as solid adsorbents, J. Hazard. Mater. 184 (2010) 477–484. https://doi.org/http://dx.doi.org/10.1016/j.jhazmat.2010.08.059.

[18] N.A.S. Amin, J. Akhtar, H.K. Rai, Screening of combined zeolite-ozone system for phenol and COD removal, Chem. Eng. J. 158 (2010) 520–527. https://doi.org/http://dx.doi.org/10.1016/j.cej.2010.01.042.

[19] B. Koubaissy, G. Joly, P. Magnoux, Adsorption and Competitive Adsorption on Zeolites of Nitrophenol Compounds Present in Wastewater, Ind. Eng. Chem. Res. 47 (2008) 9558–9565. https://doi.org/10.1021/ie8001777.

[20] D.W. Breck, E.M. Flanigen, Synthesis and properties of Union Carbide zeolites L, X and Y, in: Mol. Sieves, Society of Chemical Industry, 1968: pp. 28–38.

[21] S. Morin, P. Ayrault, N.S. Gnep, M. Guisnet, Influence of the framework composition of commerical HFAU zeolites on their activity and selectivity in m-xylene transformation, Appl. Catal. A Gen. 166 (1998) 281–292. https://doi.org/http://dx.doi.org/10.1016/S0926-860X(97)00263-9.

[22] A. Klinkenberg, Heat Transfer in Cross-Flow Heat Exchangers and Packed Beds, Ind. Eng. Chem. 46 (1954) 2285–2289. https://doi.org/10.1021/ie50539a021.

[23] Y. Taamneh, R. Al Dwairi, The efficiency of Jordanian natural zeolite for heavy metals removal, Appl. Water Sci. 3 (2013) 77–84. https://doi.org/10.1007/s13201-012-0061-2.

[24] A. Chatterjee, S. Schiewer, Multi-resistance kinetic models for biosorption of Cd by raw and immobilized citrus peels in batch and packed-bed columns, Chem. Eng. J. 244 (2014) 105–116. https://doi.org/https://doi.org/10.1016/j.cej.2013.12.017.

[25] P.P. Pescarmona, K.P.F. Janssen, C. Delaet, C. Stroobants, K. Houthoofd, A. Philippaerts, C. De Jonghe, J.S. Paul, P.A. Jacobs, B.F. Sels, Zeolite-catalysed conversion of C3 sugars to alkyl lactates, Green Chem. 12 (2010) 1083–1089. https://doi.org/10.1039/b921284a.

[26] T. Beutel, M.J. Peltre, B.L. Su, Interaction of phenol with NaX zeolite as studied by 1H MAS NMR, 29Si MAS NMR and 29Si CP MAS NMR spectroscopy, Colloids Surfaces A Physicochem. Eng. Asp. 187–188 (2001) 319–325. https://doi.org/http://dx.doi.org/10.1016/S0927-7757(01)00647-1.

[27] D. Smart, T. Curtin, T.F. O'Dwyer, Influence of Cation-Exchanged Copper on the Adsorption of Phenol onto Zeolite Beta, Adsorpt. Sci. Technol. 32 (2014) 635–646. https://doi.org/10.1260/0263-6174.32.8.635.

[28] H. Jabraoui, I. Khalil, S. Lebègue, M. Badawi, Ab initio screening of cation-exchanged zeolites for biofuel purification, Mol. Syst. Des. Eng. 4 (2019) 882–892. https://doi.org/10.1039/C9ME00015A.

[29] N.Y. Chen, Hydrophobic properties of zeolites, J. Phys. Chem. 80 (1976) 60–64. https://doi.org/10.1021/j100542a013.

[30] M. Khalid, G. Joly, A. Renaud, P. Magnoux, Removal of Phenol from Water by Adsorption Using Zeolites, Ind. Eng. Chem. Res. 43 (2004) 5275–5280. https://doi.org/10.1021/ie0400447.

[31] N. Jiang, R. Shang, S.G.J. Heijman, L.C. Rietveld, High-silica zeolites for adsorption of organic micro-pollutants in water treatment: A review, Water Res. 144 (2018) 145–161. https://doi.org/https://doi.org/10.1016/j.watres.2018.07.017.

[32] H.S. Cerqueira, G. Caeiro, L. Costa, F. Ramôa Ribeiro, Deactivation of FCC catalysts, J. Mol. Catal. A Chem. 292 (2008) 1–13. https://doi.org/https://doi.org/10.1016/j.molcata.2008.06.014.

[33] F. Hernández-Beltrán, J.C. Moreno-Mayorga, M. de Lourdes Guzmán-Castillo, J. Navarrete-Bolaños, M. González-González, B.E. Handy, Dealumination–aging pattern of REUSY zeolites contained in fluid cracking catalysts, Appl. Catal. A Gen. 240 (2003) 41–51. https://doi.org/https://doi.org/10.1016/S0926-860X(02)00433-7.

TABLES

Table 1. Physicochemical characteristics of the different Y zeolites used in this study.

Zeolites	Unit cell formula	Na (wt.%) [a]	Si/Al [b]	Si/Al_{IV} [c]	Si/Al_{IV} NMR [d]	Particle size (µm) [e]
DAY P	$H_{1.9}Al_{1.9}Si_{190.1}O_{384}$	0.0	100	-	-	6.2
$Na_{2.1}$USHY	$Na_{17.5}H_{20.9}Al_{38.4}Si_{153.6}O_{384}$; 16.5 EFAL	2.1	2.8	4.0	-	4.4
$Na_{3.0}$USHY	$Na_{24.6}H_{16.3}Al_{40.9}Si_{151.1}O_{384}$; 13.1 EFAL	3.0	2.8	3.7	-	-
CBV 720	$H_{11.3}Al_{11.3}Si_{180.7}O_{384}$; 0.8 EFAL	0.0	15	16	22	4.4
CBV 780	$H_{4.9}Al_{4.7}Si_{187.3}O_{384}$	0.0	40	40	40.4	-

CBV 600	$H_{18.9}Al_{18.8}Si_{173.2}O_{384}$; 47.8 EFAL	0.0	2.6	9.2	9.6	4.6
CBV 500	$H_{40}Al_{40}Si_{152}O_{384}$; 14.4 EFAL	0.0	2.9	3.8	4.6	-

[a]from elemental analysis; [b]from manufacturer; [c]framework Si/Al_{IV} ratio calculated from the unit cell parameter a_0 (PXRD experiments), using Breck–Flanigen equation [20], [d]from P. P. Pescarmona *et al.* [25], [e]measured by laser diffraction.

Table 2. Textural and acidity properties of the Y zeolite samples.

Sample	Pore size (Å)	S_{ext} ($m^2.g^{-1}$)	Pore volume ($cm^3\,g^{-1}$)[a]		Acidity (μmol g^{-1})[b]		
			V_{micro}	V_{meso}	Brønsted	Lewis	Total
DAY P	58	36	0.30	0.06	24	23	47
$Na_{2.1}$USHY	159	15	0.29	0.04	416	373	789
$Na_{3.0}$USHY	162	17	0.29	0.06	453	225	678
CBV 720	242	84	0.31	0.21	281	122	403
CBV 780	240	83	0.33	0.18	39	101	140
CBV 600	159	56	0.24	0.13	271	396	667
CBV 500	161	33	0.28	0.08	628	343	971

[a]V_{micro} from *t*-plot, $V_{meso} = V_{total} - V_{micro}$; [b]from pyridine desorption at 150 °C.

Table 3. $t_{5\%}$, $t_{95\%}$, Q_T, breakthrough curves slopes, k_a and K_e parameters obtained from Klinkenberg model fittings [22].

Sample	$t_{5\%}$ (min)	$t_{95\%}$ (min)	Slope (min^{-1})	Q_T (mmol g^{-1})	k_a (min^{-1})	K_e ($x10^3$)
DAY P	10	19	0.100	0.40	3.70	3.0
$Na_{2.1}$USHY	49	86	0.024	1.82	1.04	13.8
$Na_{3.0}$USHY	50	87	0.024	1.86	1.10	14.1
CBV 720	22	43	0.043	0.87	1.65	6.6
CBV 780	17	34	0.053	0.68	1.79	5.2
CBV 600	29	47	0.050	1.05	2.60	7.9
CBV 500	35	77	0.021	1.51	0.69	11.4

Figures captions

Figure 1. Nitrogen sorption isotherms (A) and PSD curves (B) for the different zeolite samples (□ DAY P, ∇ $Na_{3.0}$USHY, o $Na_{2.1}$USHY, Δ CBV 500 ◄ CBV 720, ■ CBV 780 and ● CBV 600).

Figure 2. Total (Δ) and Brønsted (○) acidity as a function of, respectively, global and framework Si/Al (A); Lewis (□) acidity as a function of EFAL species (B).

Figure 3. Breakthrough curves (guaiacol adsorption) obtained for DAY P (A) and $Na_{2.1}$USHY (B) samples.

Figure 4. Amount of guaiacol adsorbed (Q_T) as a function of parameter K_e.

Figure 5. Slope of the breakthrough adsorption curves as a function of parameter k_a.

Figure 6. Amount of guaiacol adsorbed as a function of global Si/Al ratio (A) and Al molar percentage (B).

Figure 7. Amount of guaiacol adsorbed (Q_T) as a function of Brønsted acidity.

Figure 8. Amount of guaiacol adsorbed (Q_T) as a function of Lewis acidity (A) and EFAL species (B).

Figure 9. Amount of guaiacol adsorbed Q_T as a function of the mesopores volume V_{meso} (inset: V_{meso} as a function of external surface area, S_{ext}).